Journal of Medicinal Chemistry

Drug Annotation

3-[(1*S*,2*S*,3*R*)-2,3-Difluoro-1-hydroxy-7-methylsulfonyl-indan-4-yl]oxy-5-fluoro-benzonitrile (PT2977), a Hypoxia-Inducible Factor 2# (HIF-2#) Inhibitor for the Treatment of Clear Cell Renal Cell Carcinoma

Rui Xu, Keshi Wang, James P. Rizzi, Heli Huang, Jonas A. Grina, Stephen T. Schlachter, Bin Wang, Paul M. Wehn, Hanbiao Yang, Darryl D. Dixon, Robert M. Czerwinski, Xinlin Du, Emily L. Ged, Guangzhou Han, Huiling Tan, Tai Wong, Shanhai Xie, John A. Josey, and Eli M. Wallace

J. Med. Chem., **Just Accepted Manuscript** • DOI: 10.1021/acs.jmedchem.9b00719 • Publication Date (Web): 24 Jun 2019

Just Accepted

is published by the American Chemical Society. 1155 Sixteenth Street N.W., Washington, DC 20036

3-[(1*S*,2*S*,3*R*)-2,3-Difluoro-1-hydroxy-7-methylsulfonyl-indan-4-yl]oxy-5-fluoro-benzonitrile (PT2977), a Hypoxia-Inducible Factor 2α (HIF-2α) Inhibitor for the Treatment of Clear Cell Renal Cell Carcinoma

Rui Xu,*† Keshi Wang,† James P. Rizzi, Heli Huang, Jonas A. Grina, Stephen T. Schlachter,‡ Bin Wang, Paul M. Wehn, Hanbiao Yang, Darryl D. Dixon,# Robert M. Czerwinski, Xinlin Du, Emily L. Ged, Guangzhou Han, Huiling Tan, Tai Wong, Shanhai Xie, John A. Josey, Eli M. Wallace

Peloton Therapeutics, Inc., 2330 Inwood Road, Suite 226, Dallas, TX 75235

† These authors contribute equally

ABSTRACT

The hypoxia-inducible factor 2α (HIF-2α) is a key oncogenic driver in clear cell renal cell carcinoma (ccRCC). Our first HIF-2α inhibitor PT2385 demonstrated promising proof of concept clinical activity in heavily pretreated advanced ccRCC patients. However, PT2385 was restricted by variable and dose-limited pharmacokinetics resulting from extensive metabolism of PT2385 to its glucuronide metabolite. Herein we describe the discovery of second-generation HIF-2α inhibitor PT2977 with increased potency and improved pharmacokinetic

profile achieved by reduction of phase 2 metabolism. Structural modification by changing the geminal difluoro group in PT2385 to a vicinal difluoro group resulted in enhanced potency, decreased lipophilicity and significantly improved pharmacokinetic properties. In a phase 1 dose-escalation study, the clinical pharmacokinetics for PT2977 supports the hypothesis that attenuating the rate of glucuronidation would improve exposure and reduce variability in patients. Early evidence of clinical activity shows promise for PT2977 in the treatment of ccRCC.

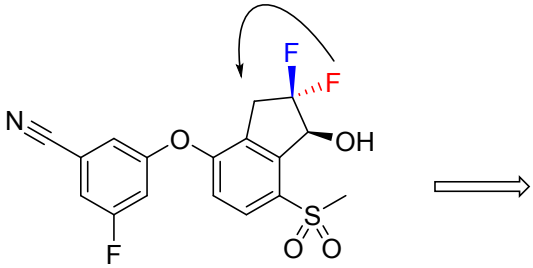

1
(PT2385)

$LogD_{7.4}$: 2.2
VEGFA EC_{50}: 46 nM
Human PPB: 82% bound
Free fraction adjusted EC_{85}: 540 ng/mL

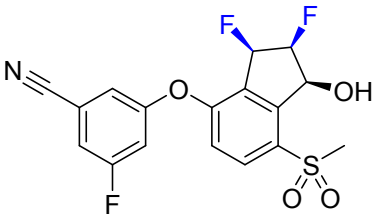

2
(PT2977)

$LogD_{7.4}$: 1.2
VEGFA EC_{50}: 17 nM
Human PPB: 52% bound
Free fraction adjusted EC_{85}: 75 ng/mL

INTRODUCTION

Kidney cancer is among the 10 most common cancers in both men and women. Nearly 74,000 new cases of kidney cancer are estimated to be diagnosed in the United States in 2019 with over 14,000 deaths.[1] Clear cell renal cell carcinoma (ccRCC) is the most common form of kidney cancer. Although targeted therapies and immunotherapies have considerably improved the prognosis for patients with ccRCC,[2] only 12% of patients with advanced or metastatic disease

will survive 5 years.[3] There exists a significant medical need for better therapeutic options for ccRCC patients with metastatic disease.

In the majority of patients, ccRCC is characterized by inactivation of the tumor suppressor von Hippel-Lindau (VHL) due to genetic predisposition, somatic mutations or methylation.[4,5] The VHL protein (pVHL) is a component of an E3 ubiquitin ligase complex that mediates protein degradation by the proteasome. A principal role of pVHL is the regulation of the hypoxia-inducible factor (HIF) family of transcription factors consisting of HIF-1α, HIF-2α, and the less well characterized HIF-3α.[6-9] Unlike HIF-1α, in adults the expression of HIF-2α is limited to endothelial cells, kidney fibroblasts, hepatocytes, intestinal lumen epithelial cells, pancreatic interstitial cells, heart myocytes, interstitial cells, and lung type II pneumocytes.[10,11] Importantly, HIF-2α activity has been demonstrated to be a key oncogenic driver in ccRCC.[12-15] In mouse ccRCC tumor models, knockdown of HIF-2α expression in pVHL defective cell line blocked tumor growth comparable to reintroduction of pVHL. In addition, expression of a stabilized variant of HIF-2α was able to overcome the tumor suppressive role of pVHL. HIF-2α has also been shown to contribute to tumorigenesis in other malignancies such as glioblastoma multiforme where hypoxia is a key feature of the tumor microenvironment and a correlation between HIF-2α activity and survival has been observed.[16,17]

The activity of HIF-2α is controlled by oxygen-dependent hypoxia-inducible factor prolyl-hydroxylases (PHDs).[18,19] When oxygen availability is high (normoxia), these enzymes hydroxylate specific proline residues on the oxygen-dependent domain of HIF-2α, creating a substrate recognition site for pVHL. pVHL recognizes the modified form of HIF-2α, binds to it and targets it for rapid proteasomal degradation. Under hypoxic conditions, there is insufficient

oxygen for the PHDs to catalyze hydroxylation of HIF-2α, and pVHL cannot bind unmodified HIF-2α. As a result, HIF-2α accumulates and translocates to the nucleus where it dimerizes with the constitutively expressed aryl hydrocarbon receptor nuclear translocator (ARNT, also known as HIF-1β) to form an active transcription factor complex. This complex recognizes hypoxia-responsive elements (HRE) on DNA leading to increased expression of a variety of proteins, many of which coordinately regulate angiogenesis, proliferation, migration and immune evasion.[20-22] In ccRCC, pVHL is defective or absent in the vast majority of patients which leads to the accumulation and transcriptional activation of HIF-2α even under normoxic conditions. While many gene products involved in the hypoxic response have been explored individually as therapeutic targets for cancer, broad inhibition of the pathway through direct targeting of HIF-2α offers an exciting opportunity to attack tumors on multiple axes.[22]

Despite the inherent difficulties in targeting DNA binding transcription factors, groundbreaking research demonstrated that small molecule binding to an inner pocket in HIF-2α could allosterically inhibit the protein-protein interaction between HIF-2α and ARNT leading to inhibition of transcriptional activity.[23-26] In a previous report,[27] we disclosed our efforts guided by iterative structure-based drug design and rational modification to identify a novel series of HIF-2α inhibitors with excellent potency and physical and pharmacologic properties. This work led to the discovery of compound **1** (PT2385), the first HIF-2α inhibitor to enter clinical development.[28-30] Although PT2385 was associated with highly variable drug exposure, anti-tumor activity was observed in heavily pretreated advanced ccRCC patients, providing HIF-2α target validation.[31] Herein we describe the path from PT2385 to the clinical candidate compound **2** (PT2977) by optimizing potency and DMPK properties.

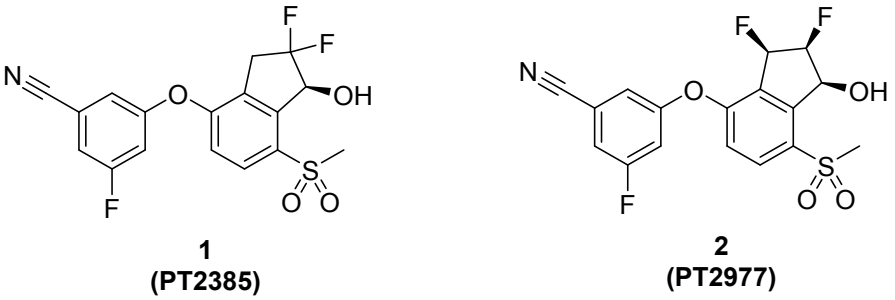

Figure 1. Structures of compounds **1** and **2**.

BACKGROUND

A first-in-human study to evaluate PT2385 for safety, pharmacokinetics (PK) and pharmacodynamics (PD) was completed in patients with advanced ccRCC previously treated with one or more VEGF inhibitors.[31] PT2385 was administered orally at twice-per-day (b.i.d.) doses of 100 to 1800 mg, according to a standard 3 + 3 dose-escalation design, followed by an expansion phase at the recommended phase 2 dose (RP2D). The dose-escalation and expansion phases enrolled 26 and 25 patients, respectively. PT2385 was well-tolerated in this study, with no dose-limiting toxicities observed at any dose level tested. Exposure of PT2385 was variable and increased up to 800 mg b.i.d. No additional increases in compound circulating levels were observed up to the highest dose of 1800 mg b.i.d. PT2385 treatment resulted in rapid decreases in plasma erythropoietin (EPO), a HIF-2α regulated gene, at all doses, demonstrating target engagement and biological activity. No further reduction was observed above 800 mg b.i.d. Based on safety, PK, and PD data, 800 mg b.i.d. was recommended as the phase 2 dose. PT2385 demonstrated promising anti-tumor activity in these heavily pretreated patients. Of the 47

evaluable patients, one patient had a complete response (CR), six patients had a partial response (PR), and 26 patients had stable disease (SD). Three patients remained in the study for over 3 years. Statistical analyses were performed to determine the relationship between PK parameters and anti-tumor activity of PT2385. PT2385 steady-state trough level was found to be significantly correlated with progression free survival (PFS). Patients with PT2385 trough concentrations greater than 500 ng/mL experienced improved PFS (14.3 months) compared to patients with PT2385 levels below 500 ng/mL (1.4 months) (Figure 2). PT2385 plasma concentration of 500 ng/mL is equivalent to the free-fraction adjusted EC_{85} in the vascular endothelial growth factor A (VEGFA) secretion assay in 786-O cells, a VHL-mutant ccRCC cell. In the 786-O mouse xenograft model, PT2385 trough plasma concentration of 500 ng/mL was also required to achieve maximum anti-tumor activity.

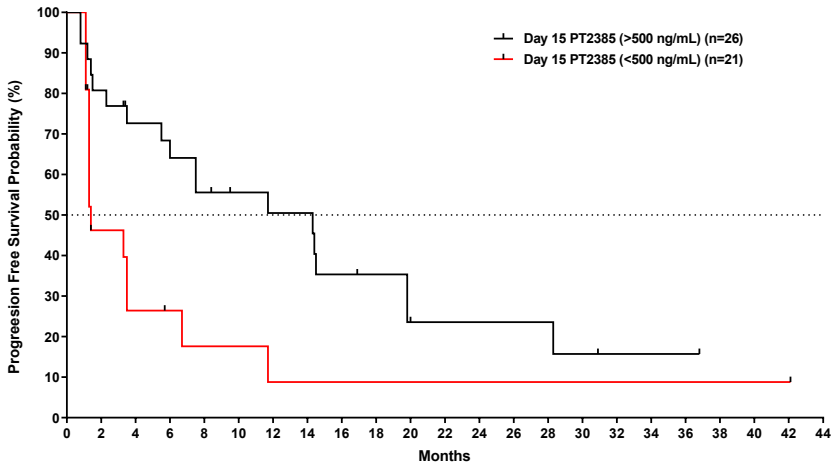

Figure 2. Comparison of progression-free survival (PFS) profiles in patients experiencing steady-state exposure trough concentrations < 500 ng/mL (red line) *versus* those with trough

concentrations > 500 ng/mL (black line). Data include all evaluable patients in dose escalation phase and expansion cohort (n = 47).

RESULTS AND DISCUSSION

PT2385 Human PK Analysis

Evaluation of the pharmacokinetic profiles of PT2385 in patients showed that a significant proportion were underexposed. Individual time-plasma concentration curves for all 25 patients who received a single 800 mg dose (the RP2D) of PT2385 shows that patients could be categorized into "normal exposure" and "low exposure" groups (Figure 3). From a total of 25 patients, 6 patients belonged to the "low exposure" group. These patients had significantly lower area under the curve (AUC) and trough plasma concentrations than those in the "normal exposure" group, and importantly, achieved little clinical benefit from PT2385 treatment.

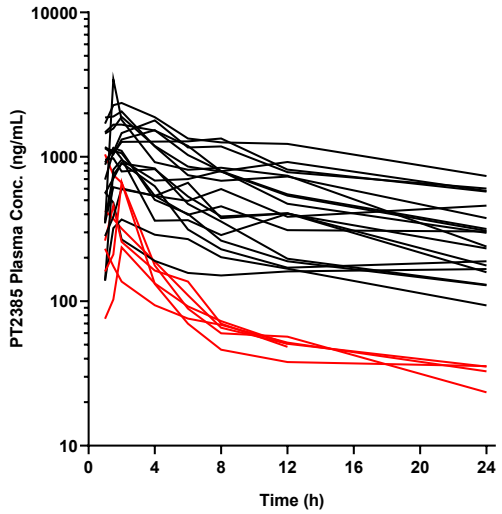

Figure 3. Concentration-time profile on day 1 for individual patients receiving 800 mg PT2385. Each line represents a separate individual who received PT2385. Red lines represent patients who had low PT2385 plasma concentrations.

The hepatic clearance of PT2385 was predicted to be low to moderate in humans with an extraction ratio (ER or observed clearance/hepatic blood flow) of 22% in human liver microsomes (HLM) and 44% in human hepatocytes. In human hepatocyte incubations, the only metabolite detectable by HPLC-UV chromatogram was the glucuronide PT2639 (Figure 4A), suggesting that the primary metabolic pathway for PT2385 in humans may be glucuronidation. The structure of PT2639 was confirmed by isolation of an authentic sample from dog urine samples after oral administration of PT2385 and chemical synthesis. In preclinical studies PT2639 did not bind to HIF-2α, with an IC_{50} greater than 100 μM in the scintillation proximity assay (SPA).[27] In the Phase 1 clinical trial, the average plasma concentration–time profiles of PT2385 and PT2639 following a single oral administration of PT2385 at 800 mg are presented in Figure 4B. The levels of PT2639 were significantly higher than PT2385. The mean AUC and C_{max} metabolite/parent ratios were 6.9 and 9.7, respectively. The high levels of PT2639 in patients was somewhat surprising based on preclinical data. While circulating levels of PT2639 were abundant in dogs (AUC ratio of PT2639:PT2385 = 1.8), it was not present in mice and was found in significantly lower levels than PT2385 in rats (AUC ratio of PT2639:PT2385 = 0.24).

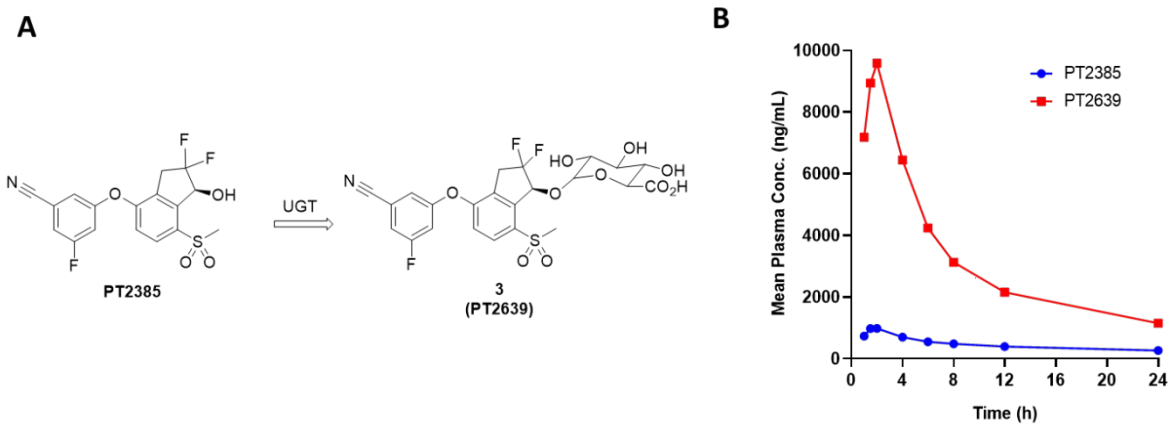

Figure 4. (A) Structure of the glucuronide metabolite **3** (PT2639). (B) Mean plasma concentration of PT2385 and PT2639 after single oral administration of 800 mg PT2385.

In the phase 1 dose escalation study, the mean AUC of PT2385 on day 1 increased with increasing dose from 100 to 800 mg in a generally dose-proportional manner, while a further increase was not achieved when escalating to 1800 mg (Figure 5A). Unlike the parent drug, its metabolite PT2639 showed more than proportional increases in exposure with higher doses (Figure 5B). For orally administered drugs, aqueous solubility is one important parameter that could contribute to inadequate and variable bioavailability. PT2385 is a BCS Class 2[32] compound with moderate thermodynamic aqueous solubility at pH 7.4 (15 µg/mL) and high permeability. In preclinical species, PT2385 exhibited good oral bioavailability in mouse, rat and dog.[27] These results combined with the fact that parent exposure plateaued at dose levels starting at 800 mg, but metabolite exposure continued to increase, suggest that limited solubility of PT2385 in gastrointestinal fluids is not the main reason for lack of dose-proportionality at higher doses. Instead, extensive, variable metabolism of PT2385 to PT2639 is likely the major factor contributing to its suboptimal pharmacokinetic profile.

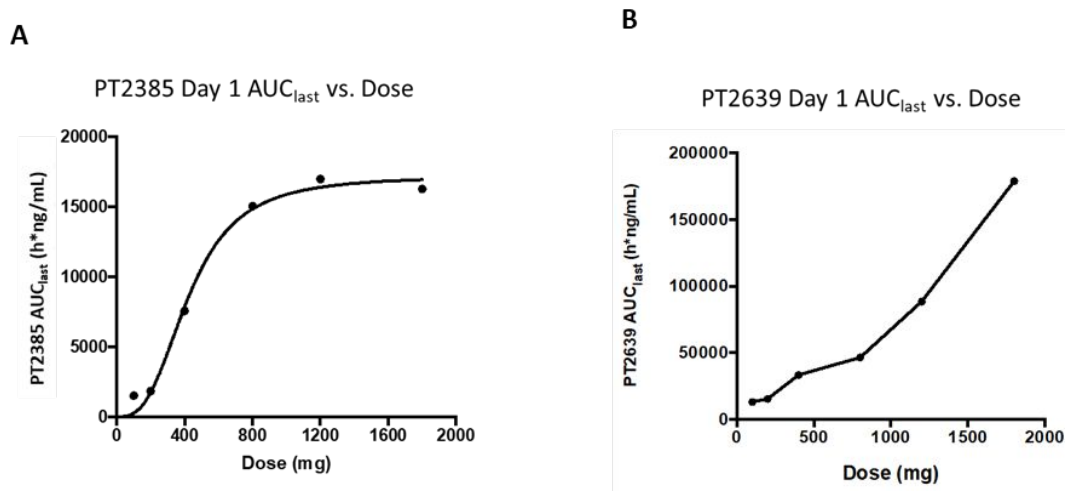

Figure 5. (A) Dose-response plot showing dose-limiting exposure of PT2385. (B) Dose-response plot showing super-proportional exposure of PT2639.

To determine which human uridine 5'-diphospho-glucuronosyltransferases (UDP-glucuronosyltransferases, or UGTs) are responsible for direct glucuronidation of PT2385, eleven recombinantly expressed UGTs were incubated with 50 μM PT2385 and the formation of PT2639 was monitored (Figure 6). Significant PT2639 was formed after 60-minute incubation with UGT2B17 supersomes, indicating PT2385 is a substrate of UGT2B17. There was none or very little PT2639 detected after incubation of PT2385 with the ten other UGTs, suggesting that UGT2B17 is the major enzyme responsible for PT2639 formation. UGT2B17 belongs to the UGT2 superfamily of UGTs and plays an important role in testosterone metabolism in humans.[33] UGT2B17 is primarily expressed in human intestine where it is found in much greater abundance than liver. It was reported that mRNA expression of UGT2B17 in the intestine is about 13-fold higher than in the liver,[34] and protein abundance in intestine is 4.4-fold higher than in liver.[35] Importantly, among all UGTs the 2B17 isoform has the highest expression in the intestine. It constitutes 59% of total UGT isoforms in the intestine but only 3% in the liver.[36] UGT2B17 is

one of the most frequently deleted genes in humans.[37] It also shows high inter-patient variability in its protein abundance in both adult human liver microsomes (HLM) and human intestine microsomes (HIM).[38] Genetic polymorphism, unique abundance in the intestine and high inter-individual expression all contribute to variable exposure for orally administered UGT2B17 metabolized drugs, likely as a result of first pass metabolism.[38,39] These data strongly suggest that gastrointestinal metabolism of PT2385 to PT2639, mediated by UGT2B17, is likely the cause of the significant variability and low drug plasma exposure in the clinic.

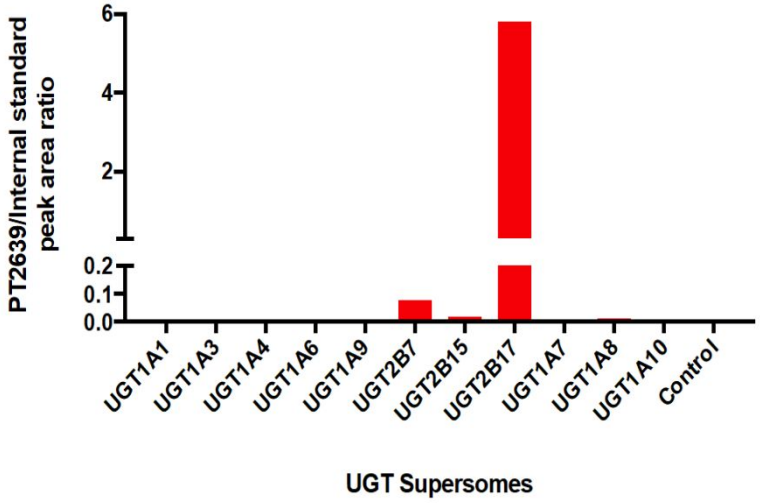

Figure 6. Formation of PT2639 by recombinant human UGTs.

We also performed studies to evaluate additional potential mechanisms responsible for dose-limiting drug exposure of PT2385 observed in patients. In small intestine, efflux transporters play important roles in the disposition of glucuronide metabolites. P-gp, BCRP and MRP2 are three major efflux transporters expressed in the small intestine.[40] The efflux ratio of PT2385 and PT2639 across MDCKII-MDR1 and MDCKII-BCRP cells was less than 2 at concentrations up

to 300 μM, suggesting that they are not substrates of P-gp or BCRP. PT2385 and PT2639 were also evaluated in the MRP2 transporter assay in membrane vesicles expressing human MRP2 protein. There was no MRP2-dependent uptake observed for PT2385. However, the MRP2 uptake of PT2639 was approximately 32-fold higher in vesicles that contained ATP compared to those without suggesting active transport. As the concentration of PT2639 was increased, uptake into MRP2-expressing vesicles plateaued suggesting active transport was saturated. The maximum velocity (V_{max}) and substrate concentration at half maximum velocity (K_m) were determined to be 1230 pmol/min/mg protein and 97 μM, respectively. The ATP dependent activity was abolished by the MRP2 inhibitor benzbromarone. These data support that PT2639 is a substrate of MRP2 and at higher concentrations PT2639 can saturate MRP2. We also have shown that PT2639 can be converted to PT2385 by bacterial β-glucuronidase *in vitro*.

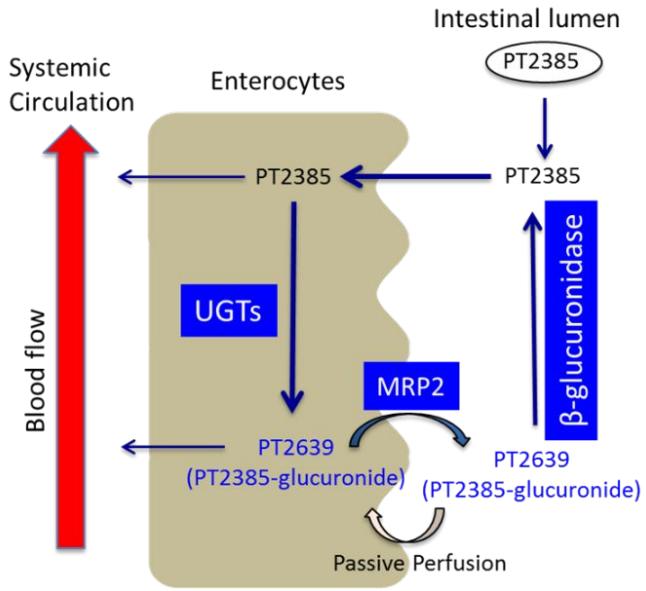

Figure 7. Proposed UGT2B17, MRP2 and β-glucuronidase interplay in the absorption of PT2385

Based on these studies and clinical pharmacokinetic data, we propose an absorption model to explain the intestinal metabolism of PT2385 that, we believe, is responsible for its suboptimal oral exposure in patients (Figure 7). After oral administration, PT2385 is absorbed through the enterocytes by passive transcellular diffusion. A small portion of PT2385 is transported to the blood as parent, while the rest of the drug is extensively metabolized by UGT2B17 to form PT2639. PT2639 can then follow one of two routes; absorption into the blood stream or active MRP2-mediated transport to the intestinal lumen. Once in the gastrointestinal lumen, PT2639 can then be converted by the action of bacterial β-glucuronidase to PT2385, which can undergo intestinal re-absorption resulting in a re-circulation cycle. Additional data to support this model includes PT2639 dog PK. After intravenous (i.v.) and oral gavage (p.o.) administration of PT2639 to dogs, significant levels of PT2385 were generated by both routes, with oral dosing generating more PT2385 than i.v. dosing.

This proposed mechanism involves UGT2B17, MRP2 and β-glucuronidase functioning individually and working in concert. The genetic polymorphism and irregular expression of these three components likely all play roles in the observed variable exposure of PT2385. Finally, the local enterocyte concentration of PT2639 generated by UGT2B17 after oral doses of PT2385 greater than 800 mg likely surpassed the K_m of PT2639 for MRP2, resulting in saturation of the transporter and thus dose-limited exposure of PT2385 and super-proportional exposure of PT2639. Therefore, the preclinical and clinical PT2385 and PT2639 data supports our model, and provides a framework for medicinal chemistry optimization to overcome PT2385 pharmacokinetic liabilities.

Compound Design and Lead Optimization

Despite the complexity of our proposed model, the pharmacokinetic issues with PT2385 may all relate to extensive metabolism of PT2385 to PT2639 by UGT2B17 in the intestine. Thus, our primary strategy to enhance HIF-2α inhibition in patients was to reduce formation of the glucuronide metabolite while retaining potency, selectivity and pharmacological profile of PT2385.

Glucuronidation is an important pathway of human drug metabolism. Most often glucuronidation is the second step of drug metabolism by acting on hydroxylated products generated by oxidative metabolism. However, it can also react directly with drugs containing hydroxyl, carboxylic acid, amino or thiol functional groups. Glucuronidation is a S_N2 reaction catalyzed by the UGT enzymes in which the metabolized or parent drug acts as a nucleophile, the secondary alcohol in the case of PT2385, and the cofactor UDP-α-*D*-glucuronic acid (UDPGA, **4**) as the electrophile (Figure 8). The rate of glucuronidation is dependent on both nucleophilicity and the steric environment of the drug. For *O*-glucuronidation, deprotonation of the alcohol is considered to be a key step.[41-43] Alcohols substituted by electron withdrawing groups tend to have lower pK_a, and thus higher reactivity in the glucuronidation reaction.

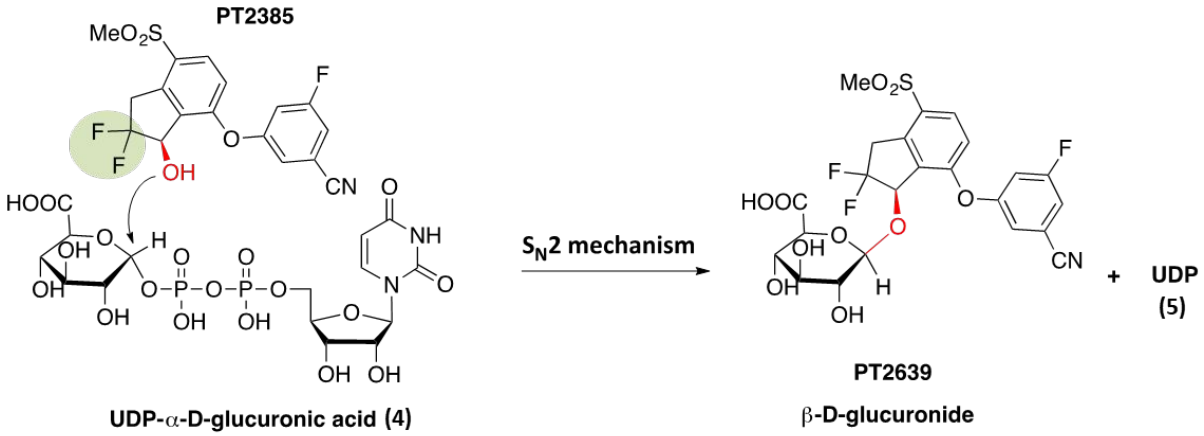

Figure 8. Glucuronidation reaction of PT2385

Previously,[27] we described the discovery of a series of indanols as potent and selective inhibitors of HIF-2α. Protein-inhibitor X-ray crystal structure of PT2385 as shown in Figure 9 revealed two key protein-ligand interactions. The hydroxyl group in PT2385 engages a hydrogen bonding network with Tyr281, a bound water molecule and His293. Three residues in HIF-2α, Met252, His293 and Tyr278 must move to accommodate the formation of this hydrogen bonding network. These movements lead to highly unfavorable steric clash between Tyr278 in HIF-2α and Phe446 in ARNT, resulting in HIF-2α:ARNT dimer disruption and inhibition of HIF-2α transcriptional activity. Another key interaction between the ligands and HIF-2α is a putative n $\rightarrow \pi^*_{Ar}$ type of interaction[44] between the phenolic oxygen of Tyr281 and the centroid of the benzene portion of the indane ring. Maintaining an electron deficient ring system is critical to engage this interaction for optimum ligand binding. The electron-withdrawing methyl sulfone group in PT2385 enhances binding affinity by decreasing the electron density of the benzene ring.

Due to the importance of the hydroxyl group to dimer disruption, cellular potency and physical properties, our design strategy for the second-generation HIF-2α inhibitors was to maintain the hydroxyl group, but significantly reduce its reactivity in glucuronidation and thereby improve pharmacokinetic performance. The geminal difluoro group in the indanol series provides a 10 to 20-fold enhancement of cell potency compared to unsubstituted analogs. We speculated that the *cis*-fluorine atom engages in intramolecular C−F···H−O electrostatic interactions and thus reduce the desolvation penalty required for ligand binding.[27,45] However, the highly electronegative fluorine atoms, through a strong inductive effect, also likely increase the hydroxyl moiety's reactivity in the glucuronidation reaction. In order to compensate for the

likely decreased activity of analogs without the geminal difluoro group, additional optimization was required to identify potency enhancing moieties.

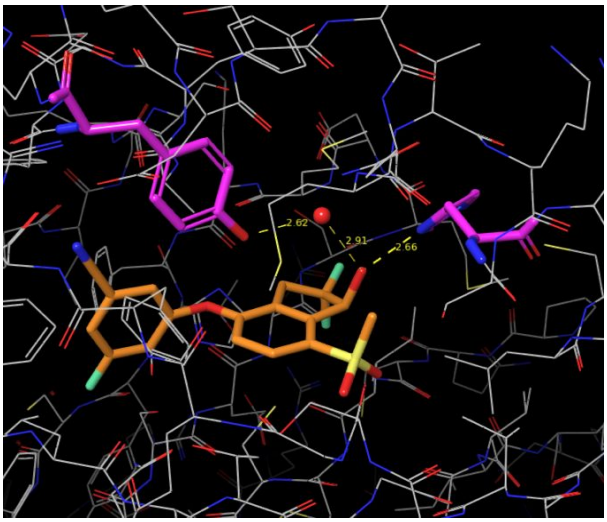

Figure 9. X-ray crystal structure of PT2385 (in orange) in complex with the HIF-2α PAS-B*/ARNT PAS-B* dimer (PDB:5TBM).[27] Tyr281 and His293 are highlighted (magenta). Dotted lines indicate hydrogen bond interactions and the red sphere denotes a water molecule

Based on our understanding of the key n → π^*_{Ar} type of interaction between the phenolic oxygen of Tyr281 and the small molecule ligands, we hypothesized that introducing a fluorine group at the benzylic position of PT2385 may further decrease the electron density of the phenyl ring resulting in a stronger n → π^*_{Ar} electrostatic interaction and increased potency. A series of compounds with fluorine substitution on the indanol ring were prepared and tested in the SPA binding assay as well as HIF-2α luciferase assay in 786-O cells. As summarized in Table 1, removal of the geminal difluoro group in PT2385 (compound **6**) led to 8-fold decrease of potency in the biochemical assay and 30-fold decrease of potency in the cellular assay, consistent with the previous SAR. One particularly interesting finding that emerged from mono-fluorine

substitution on the 2-position of the indanol core is the different potency profiles between compounds with *cis* and *trans* configurations. The *cis*-fluorohydrin **7** retained most of the potency of PT2385, with EC_{50} within 2-fold of PT2385 in the luciferase assay. On the contrary, the *trans*-fluorohydrin **8** was more than 10-fold less potent than **7**. Mono-fluorination at the benzylic position resulted in even more dramatic potency differences between the two diastereomers. While the *cis*-diastereomer **9** was 2-fold more potent than **6** in the luciferase assay, introduction of a fluorine atom with *trans*-configuration at the benzylic position completely abrogated binding affinity (compound **10**). Combination of the two fluorine atoms at *cis* relative configuration to the hydroxyl group resulted in potency improvement in a synergistic manner. Compound **2** was about 2-fold more potent than PT2385 in the luciferase assay. Reverting the fluorine stereochemistry at the benzylic position again decreased potency. Compound **11** was almost 200-fold less potent than **2** in both the binding and cellular assays. Weak activity for compounds with *trans*-fluorine at the benzylic position was also observed in compound **12**, which has a geminal difluoro group at the benzylic position. Inspection of the X-ray crystal structures of these analogs revealed that the benzylic *trans*-fluorine would probably point to His248, resulting in detrimental steric and electronic interactions. Finally, the trifluoro compound **13** was the most potent compound in this group. This was predicted by favorable electrostatic interactions between the geminal difluoro group with the alcohol, and the additional inductive effects on the phenyl ring from the benzylic *cis*-fluorine atom.

Table 1. SAR of substituted indanols

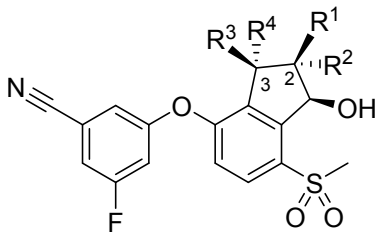

Compounds	R^1	R^2	R^3	R^4	SPA IC_{50} (μM)	Luciferase EC_{50} (μM)
1 (PT2385)	F	F	H	H	0.012 ± 0.005	0.027 ± 0.006
6	H	H	H	H	0.16 ± 0.03	0.93 ± 0.37
7	F	H	H	H	0.041 ± 0.007	0.039 ± 0.021
8	H	F	H	H	0.35 ± 0.03	0.49 ± 0.04
9	H	H	F	H	0.21 ± 0.11	0.46 ± 0.04
10	H	H	H	F	>10 (n=1)	NT
2 (PT2977)	F	H	F	H	0.009 ± 0.005	0. 011 ± 0.004
11	F	H	H	F	1.9 ± 0.3	1.9 ± 0.4
12	H	H	F	F	6.5 (n=1)	NT
13	F	F	F	H	0.009 ± 0.002	0.004 ± 0.001

To explore the effect of fluorination on the rate of glucuronidation, compounds **1**, **2**, **6-9** and **13** were evaluated in enzyme kinetic studies in HIM and UGT2B17 supersomes. The corresponding glucuronide metabolites were prepared by chemical synthesis and used as standards for quantification. Substrate saturation plots for the formation of glucuronide metabolites from parents are shown in Figure 11. Data were fitted using the Michaelis-Menten equation. Enzyme kinetics parameters V_{max} and K_m are summarized in Table 2. For PT2385, enzyme kinetics appeared to follow simple hyperbolic Michaelis-Menten kinetics with V_{max} values of 49 and 280

pmol/min/mg protein, and K_m values of 20 and 11 μM in HIM and recombinant UGT2B17, respectively. As expected, compound **13** with the geminal difluoro and benzylic fluoro groups had the highest rate of glucuronidation as determined by highest V_{max} and lowest K_m values in both systems. Surprisingly, the compound with the third highest glucuronidation rate was the *trans*-fluorohydrin compound **8**. The V_{max} of **8** was about 5-times of the corresponding *cis*-diastereomer **7** in HIM and 4-times in UGT2B17 supersomes. In a recent paper,[45] the influence of fluorination on H-bond acidity was investigated using the conformationally restricted 4-*tert*-butylcyclohexanol model. It was demonstrated that *cis*-fluorination on the α or β carbon of the cyclohexanol can significantly attenuate alcohol H-bond acidity through intramolecular F···HO interactions. We reasoned that two geminal fluorine atoms in PT2385 probably play different roles in contributing to the reactivity of PT2385 in the glucuronidation reaction. For the *cis*-fluorine, the electron-withdrawing effect and the intramolecular F···HO electrostatic interaction cancel out each other, as evident in similar glucuronidation rates between the *cis*-fluorohydrin **7** and the nonfluorinated analog **6**. In the *trans*-diastereomer, such an intramolecular hydrogen bonding interaction cannot form. As a result, the *trans*-fluorine significantly increases the acidity of the hydroxyl group in compound **8** through an inductive effect. It was also reported that 1,3-coaxial fluorohydrin in the 4-*tert*-butylcyclohexanol ring system forms a favorable F···HO interaction. Such a strong impact of 3-*cis*-fluorination was not observed in compound **9**, possibly due to a different fluorohydrin dihedral angle in the fused five-membered ring system. In compounds **2** and **7**, only the *cis*-fluorine atom that contributes positively to improved potency and decreased reactivity is maintained. Comparing to PT2385, **2** and **7** were at least 20-times slower in generating glucuronide metabolites in enzyme kinetic studies in HIM and UGT2B17 supersomes. Based on these *in vitro* results, we expect that these two compounds will afford

improved oral exposure with less variability in humans. In addition, the *cis*-benzylic fluorine in compound **2** further enhances potency. Based on potency and enzyme kinetic study results, compound **2** was selected for additional profiling.

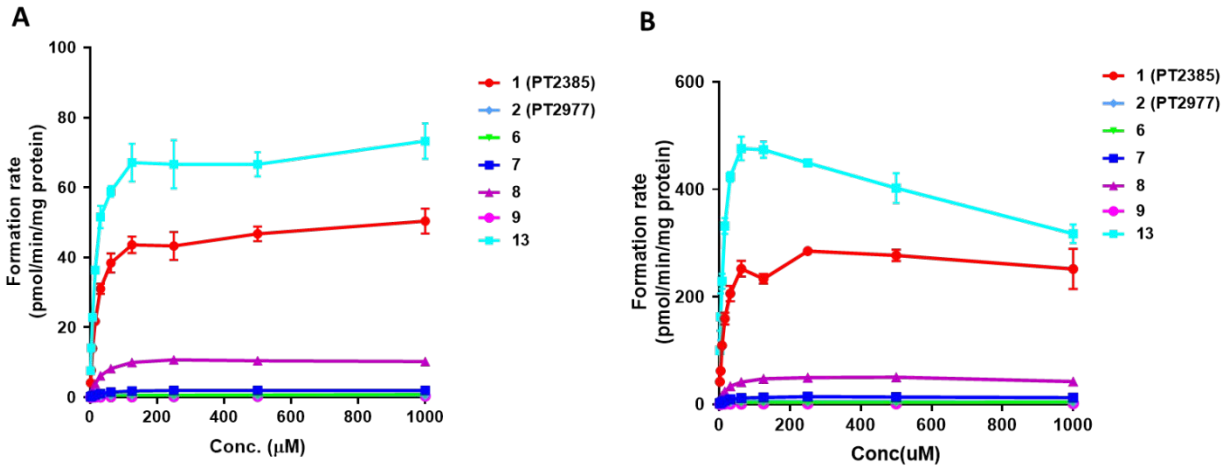

Figure 11. Substrate-concentration versus rate plots for glucuronide formation. (A) incubations in HIM; (B) incubations in UGT2B17 supersomes. The bars indicate the range of triplicate measurements.

Table 2. Enzyme kinetic parameters for the metabolism of representative indanols in human intestinal microsomes (HIM) and UGT2B17 supersomes

Compounds	HIM		UGT2B17	
	V_{max} (pmol/min/mg)	K_m (μM)	V_{max} (pmol/min/mg)	K_m (μM)
1 (PT2385)	49	20	280	11
2 (PT2977)	0.5	15	4.7	10
6	0.8	40	3.8	12
7	2.1	28	14	15
8	11	26	50	15
9	0.3	130	1.4	12
13	72	15	440	5.5

Characterization of PT2977

Compared to PT2385, PT2977 was found to be 2 to 3-fold more potent in the HIF-2α luciferase assay and the VEGFA secretion assay. Simply moving the *trans*- fluorine atom of the geminal difluoro group in PT2385 to the benzylic position with *cis*- relative configuration to the hydroxyl group resulted in significantly decreased lipophilicity. The log $D_{7.4}$ of PT2977 is about 1 log unit lower than PT2385. In general, replacement of a hydrogen with a fluorine results in slight increase in lipophilicity. However, examples have been reported in the literature that show fluorination decreases molecular lipophilicity. One extreme example is all-*cis* 1,2,3,4,5,6-hexafluorocyclohexane, a facial polarized ring reported to be one of the most polar aliphatic molecules ever measured.[46] It was also reported that compounds with fluoro substitution two or three carbons away from an oxygen atom tend to have decreased lipophilicity.[47,48] The increased polarity of PT2977 is likely due to the combination effects of fluorine atoms in close vicinity to the alcohol, and the high molecular dipole created by two vicinal electronegative fluorine atoms with *cis*-configuration. The decreased lipophilicity translates to significantly reduced plasma protein binding. PT2977 was about 30% less bound than PT2385 in the human plasma protein binding assay (52% bound *versus* 82% bound). Combining the improvement in free fraction and cellular potency, the free fraction adjusted EC_{85} for PT2977 in the VEGFA secretion assay was calculated to be 75 ng/mL. Additional profiling of PT2977 showed it to be a low clearance compound in microsomes and hepatocytes across species, and that it does not inhibit CYP P450 enzymes up to 50 μM (the highest concentration evaluated). Safety profiling of PT2977 showed low potential for QT prolongation with an estimated IC_{50} greater than 50 μM in the patch clamp hERG channel assay. It also had no appreciable activity at 10 μM in a screening panel that included 126 receptors, ion channels, kinases and phosphatases.

Table 3. *In vitro* Profile of Inhibitors PT2385 and PT2977

Compounds	PT2385	PT2977
$LogD_{7.4}$	2.2	1.2
Luciferase EC_{50} (nM)	27	11
VEGFA EC_{50} (nM)	46	17
Plasma Protein Binding (% bound in human/mouse)	82/71	52/56
Free Fraction Adjusted EC_{50} (ng/mL)	95	13
Free Fraction Adjusted EC_{85} (ng/mL)	540	75

Pharmacokinetic Profile of PT2977 in Preclinical Species

Based on its encouraging *in vitro* profile, PT2977 was evaluated in animal pharmacokinetic studies in mice, rats, dogs and monkeys. The PK profile of PT2977 after i.v. administration is summarized in Table 4. PT2977 had low plasma clearance (Cl_p) in mice, dogs and monkeys, and moderate clearance in rats. The *in vivo* hepatic extraction ratios (ER) are consistent with low to medium clearance predicted by *in vitro* stability assays in microsomes and hepatocytes, and lower potential to form glucuronide metabolite in the enzyme kinetic study.

Table 4. PK parameters of PT2977 in preclinical species after intravenous administration

Species	Dose (mg/kg)	*Vss* (L/kg)	*T1/2* (h)	*Clp* (mL/min/kg)	*in vivo* Cl *ER* (%)[c]	Microsomal *ER* (%)[c]	Hepatocyte *ER* (%)[c]
Mouse[a]	3	4.9	4.0	21	23	24	<20
Rat[b]	1	1.6	1.4	19	36	<10	33
Dog[a]	1	1.3	14	1.3	4	<10	<32
Monkey[a]	1	2.9	9.2	3.5	8	<21	<14

[a]PT2977 was delivered as a solution in 20% EtOH, 40% PEG400, 40% water. [b]PT2977 was delivered as a solution in 10% dimethylacetamide, 10% EtOH, 40%PEG400, 40% water. [c]*ER* = extraction ratio: observed clearance / hepatic blood flow.

Oral administration of PT2977 in mice, rats, dogs and monkeys resulted in good plasma exposure. Comparison of mean plasma concentration–time profiles of PT2977 and PT2385 are shown in Figure 12, and summary of parent and glucuronide metabolite drug exposure (AUC) is provided in Table 5. Interestingly, the oral exposure of PT2977 was only slightly higher than PT2385 in rodents, while these two compounds behaved very differently in higher species. The dose-normalized AUC of PT2977 was 9- and 20-fold higher than that of PT2385 AUC in dogs and monkeys, respectively. This phenomenon turned out to be related to the relative rate of glucuronide metabolite formation for each analog in these species. As shown in Table 5, the AUC of the PT2977 glucuronide metabolite (PT3317) in dogs was about 30% of the parent, while the AUC of PT2639 (PT2385 glucuronide metabolite) was almost 2-fold higher than the parent. Similarly, a low amount of circulating metabolite was observed for PT2977 in monkeys, with a metabolite/parent ratio of 0.19. Both compounds formed significantly less amounts of glucuronide metabolites in rats, suggesting an alternative metabolic pathway in this species. For PT2385, dog pharmacokinetics were a better predictor of glucuronide metabolite PT2639

formation in humans. Based on these data, we predicted that PT2977 would have a reduced propensity for glucuronidation in humans and thus demonstrate a significantly improved pharmacokinetic profile over PT2385 in patients.

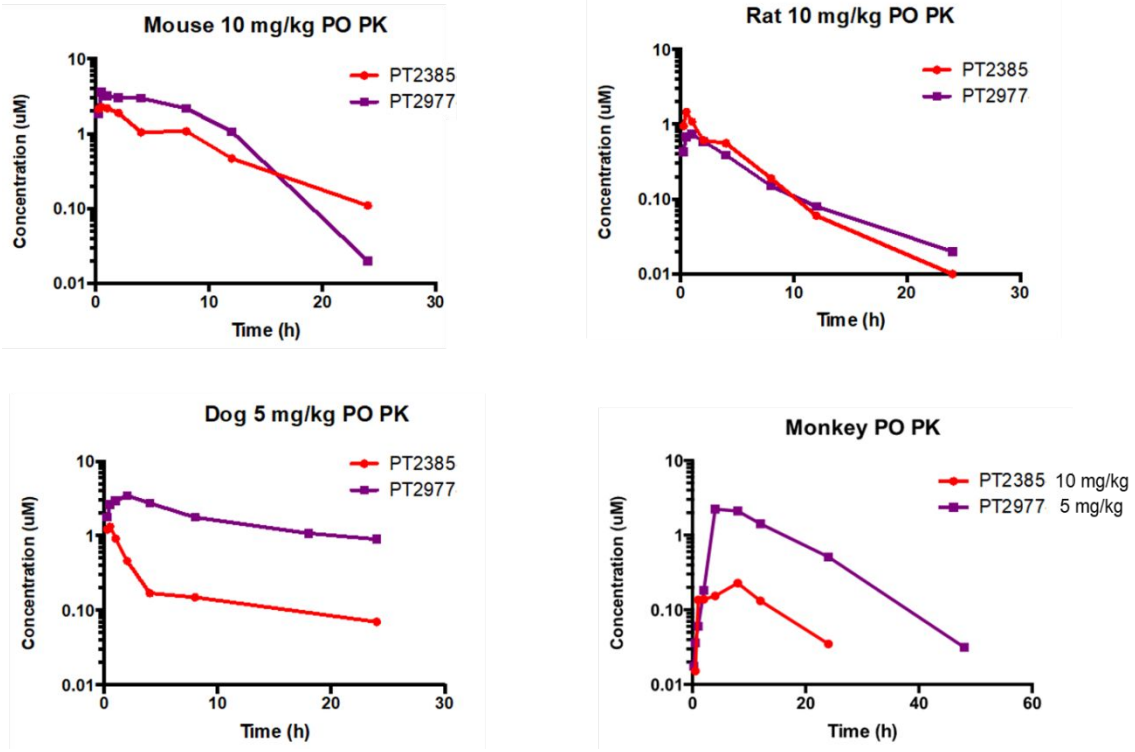

Figure 12. Mean plasma concentrations of PT2385 and PT2977 versus time in mice, rats, dogs and monkeys following single oral doses.

Table 5. Oral PK comparison between PT2385 and PT2977

Species	Compounds	Dose (mg/kg)	Parent AUC_{last} (hr* μM)	Metabolite AUC_{last} /Parent AUC_{last} (ratio)
Mouse	**PT2385**	10[a]	21	ND
	PT2977	10[a]	37	
Rat	**PT2385**	10[a]	5.1	0.24
	PT2977	10[b]	13	0.07
Dog	**PT2385**	5[b]	7.2	1.8
	PT2977	5[b]	60	0.32
Monkey	**PT2385**	10[b]	3.1	ND
	PT2977	5[b]	31	0.19

[a]PT2385 and PT2977 were delivered as a suspension in 10% EtOH, 30% PEG400, 60% (0.5% methylcellulose, 0.5% Tween 80 (aq)). [b]PT2385 and PT2977 were delivered as a suspension in 0.5% methylcellulose and 0.5% Tween 80 in water.

PK/PD Relationship and *In Vivo* Efficacy

A pharmacokinetic/pharmacodynamic (PK/PD) study was performed in mice bearing subcutaneous 786-O ccRCC tumors to correlate plasma drug levels of PT2977 with PD effects in the tumors. Six doses of PT2977 at 0.3, 1 and 3 mg/kg or PT2385 at 10 mg/kg b.i.d. were administered orally. Plasma and tumor tissue samples were collected 12 hours after the last dose. Gene expression analyses in excised tumors by qPCR showed that PT2977 potently and dose-dependently reduced mRNA levels of human cyclin D1, a target gene regulated by HIF-2α (Figure 13A). Maximum PD response was achieved at 1 mg/kg for PT2977 while a much higher dose of 10 mg/kg was required for PT2385.[28] And to achieve the same PD effect, the steady state trough plasma drug concentration of PT2977 was about 1/10 of PT2385 concentration (Figure 13B). Consistent with the improvement in potency and physical properties, compound PT2977 was about 10-fold more potent than PT2385 *in vivo*. Compound PT2977 and PT2385 were

subsequently evaluated for anti-tumor activity in the 786-O mouse xenograft model. Administration of PT2977 at 0.3, 1 and 3 mg/kg all led to rapid regression of established tumors (Figure 13C), confirming superior *in vivo* activity of compound PT2977 compared to PT2385.[28]

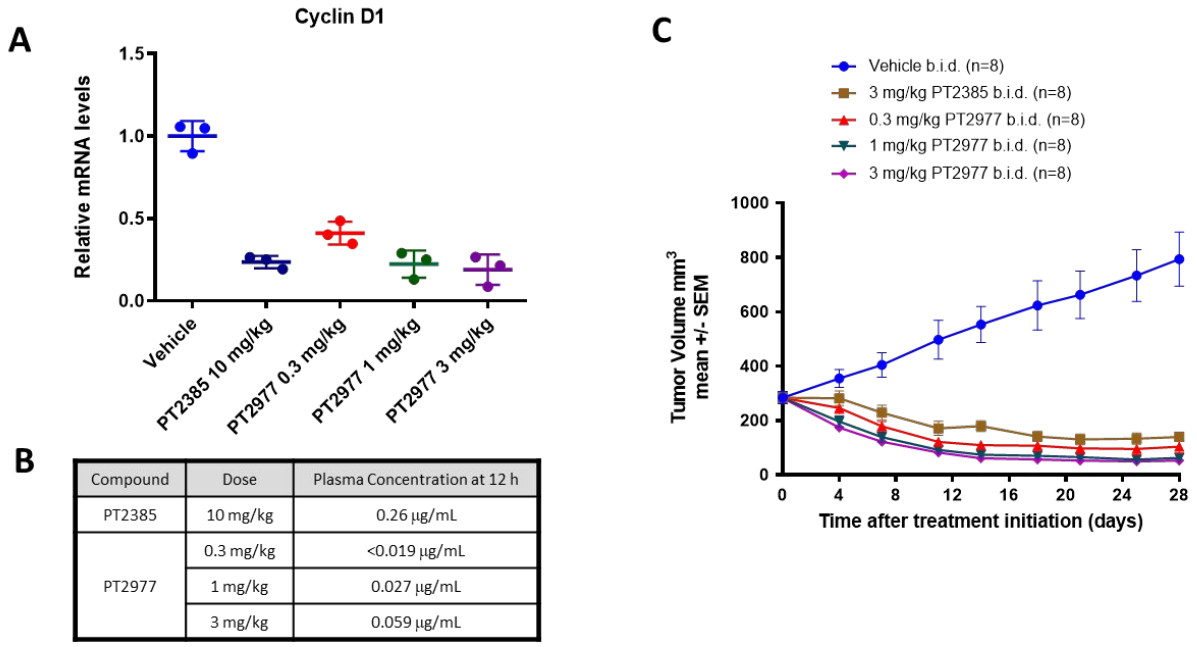

B

Compound	Dose	Plasma Concentration at 12 h
PT2385	10 mg/kg	0.26 μg/mL
PT2977	0.3 mg/kg	<0.019 μg/mL
	1 mg/kg	0.027 μg/mL
	3 mg/kg	0.059 μg/mL

Figure 13. (A) PK/PD evaluation of PT2977 and PT2385 in 786-O mouse xenograft (female SCID/beige mice, n=3) dosed at 0.3, 1 and 3 mg/kg and 10 mg/kg p.o., b.i.d., respectively. Tumors were harvested 12 hours after administration of the final dose and total RNA was isolated from the tumor samples and used to make single-stranded cDNA. The resulting cDNA was used in quantitative PCR reactions; mRNA levels were normalized to internal control cyclophilin B mRNA levels in each sample. (B) Plasma levels of PT2385 and PT2977 at 12 hours after the last dose in the PK/PD study. (C) *In vivo* efficacy study of PT2977 and PT2385 in 786-O xenografts (female SCID/beige mice, n=8).

Based on its improved potency, free fraction, pharmacokinetics and metabolite profile, compound PT2977 was predicted to have a low clinically active dose and less inter-patient

exposure varability. PT2977 was chosen as our second-generation HIF-2α clinical candidate for further investigation as a potential new treatment for ccRCC and VHL Disease.

PT2977 Phase 1 Clinical Data

In a phase 1 dose-escalation trial,[49,50] patients with advanced solid tumors were treated with PT2977 with doses ranging from 20 to 240 mg once a day. The pharmacokinetic profile on day 15 is summarized in Figure 14. Exposure of PT2977 increased with dose up to 120 mg (Table 6). Doses above 120 mg did not provide markedly increased exposure. Target steady-state trough concentration of 75 ng/mL was achieved at 20 mg and exceeded with doses at 40 mg and above.

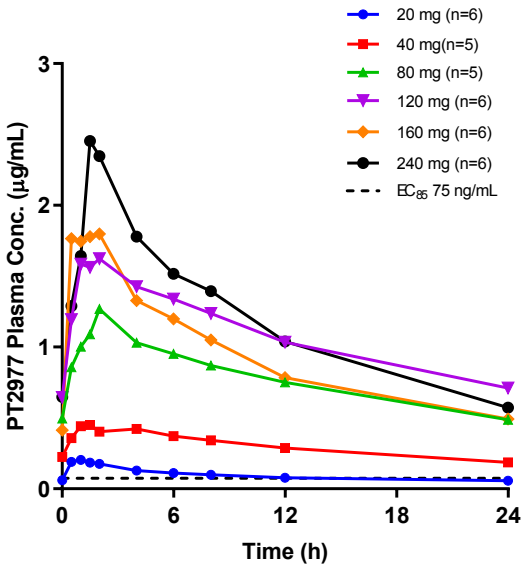

Figure 14. Mean PT2977 plasma concentration on day 15 versus time following once daily oral administration at the dose levels of 20, 40, 80, 120, 160, and 240 mg in patients with solid tumors. Dotted line denotes free fraction adjusted EC_{85} of 75 ng/mL for PT2977 in the VEGFA secretion assay in 786-O cells.

Table 6. PK parameters on day 15 following once daily oral administration of PT2977

Cohort	n	$T_{1/2}$ (h)	C_{max} (μg/mL)	AUC_{last} (h*μg/mL)	C_{24h} (μg/mL)
20 mg	6	12.5	0.2	2.1	0.06
40 mg	5	18.8	0.5	7.1	0.19
80 mg	5	15.4	1.4	17.5	0.49
120 mg	6	20.9	1.8	25.9	0.71
160 mg	6	12.2	2.0	21.0	0.49
240 mg	6	14.1	2.7	28.0	0.57

As shown in Figure 15A, treatment with PT2977 led to rapid and dose-dependent reduction in EPO expression. EPO reduction with PT2977 at 120 mg q.d. was comparable to the level of reduction in PT2385 high exposure patients (Figure 15B). PT2977 was well tolerated with anemia as the most common adverse event consistent with pharmacologic action. Maximum tolerated dose (MTD) was not reached in the phase 1 dose-escalation study. Based on PK, PD and safety data, RP2D was determined to be 120 mg q.d.

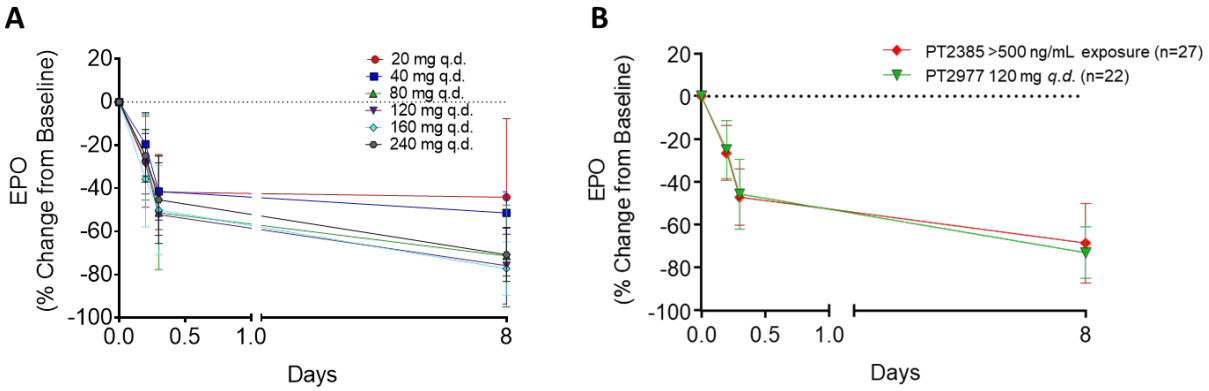

Figure 15. (A) Pharmacodynamic response as assessed by decreases in the HIF-2α target erythropoietin (EPO) following once daily oral administration of PT2977 at the dose levels of

20, 40, 80, 120, 160 and 240 mg in patients with solid tumors. (B) Decreases in EPO in high exposure PT2385 patients with > 500 ng/mL trough plasma concentration *versus* all PT2977 patients in the 120 mg cohort.

Figures 16A shows mean PT2977 and glucuronide metabolite (PT3317) plasma concentrations at steady-state *versus* time. On day 15, the trough concentration (24 h) for PT2977 at 120 mg q.d. was 500 ng/mL and the metabolite/parent ratio was 0.32. For PT2385, a 13-fold higher total daily dose was required to achieve a trough concentration of 860 ng/mL at 12 h, and the metabolite/parent ratio (6.0) was much higher than that of PT2977 (Figure 16B). In addition to greater potency and free fraction, PT2977 exposure is more consistent with no underexposed patients (Figure 17). These PK results are in-line with our prediction based on UGT2B17 enzyme kinetic data and PK in preclinical species, further supporting our hypothesis that glucuronidation plays a critical role in the absorption and metabolism of this series of HIF-2α inhibitors.

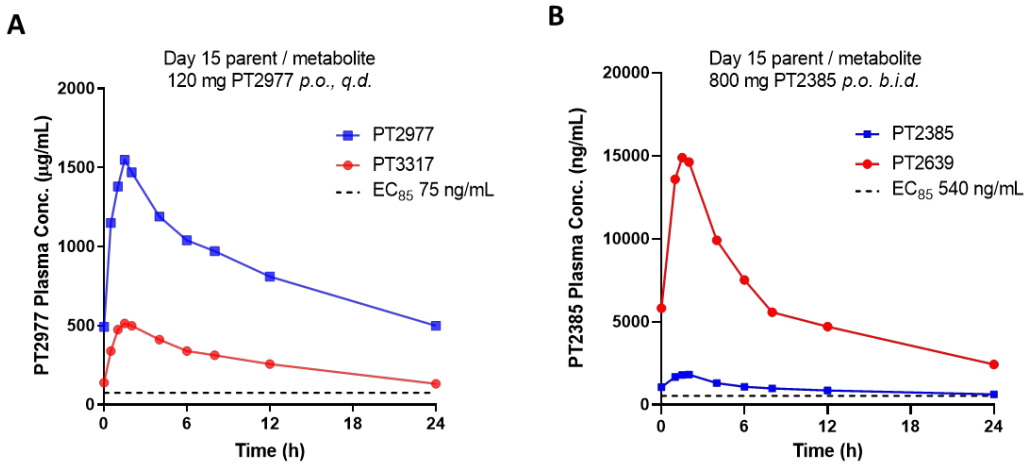

	PT2977	PT2385
Day 15 Trough	500 ng/mL (24 h)	860 ng/mL (12 h)
Metabolite/Parent AUC Ratio	0.32	6.0

Figure 16. (A) Mean PT2977 and the glucuronide metabolite PT3317 plasma concentration on day 15 *versus* time following once daily oral administration at 120 mg. Dotted line denotes free fraction adjusted EC_{85} of 75 ng/mL for PT2977 in the VEGFA secretion assay in 786-O cells. (B) Mean PT2385 and the glucuronide metabolite PT2639 plasma concentration on day 15 *versus* time following twice daily oral administration at 800 mg. Dotted line denotes free fraction adjusted EC_{85} of 540 ng/mL for PT2385 in the VEGFA secretion assay in 786-O cells. Bottom: Day 15 metabolite/parent AUC ratios and trough plasma concentrations for PT2977 and PT2385.

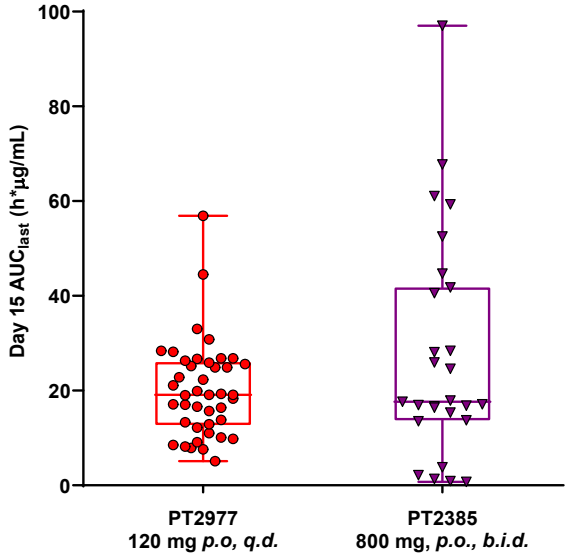

Figure 17. AUC_{last} on day 15 for individual patients received 120 mg PT2977 q.d. or 800 mg PT2385 b.i.d. Each data point represents a single patient.

CONCLUSIONS

In this paper we investigated potential causes of inter-individual PK variability and low exposure of our first-in-class HIF-2α inhibitor PT2385 in patients. Based on circulating metabolite identification and UGT phenotyping, we hypothesized that attenuating the rate of glucuronidation would improve exposure and reduce variability in patients. Structural

modification by moving one of the geminal difluoro atoms in PT2385 to the benzylic position resulted in enhanced potency, significantly decreased lipophilicity and drastically reduced glucuronidation. Enzyme kinetic studies in HIM and UGT supersomes revealed the impact of fluorine substitution and stereochemistry on rate of glucuronidation. To our knowledge, this is the first systematic study of the influence of these factors on glucuronidation. The application of fluorine in modern medicinal chemistry and drug development has expanded rapidly in recent years.[51,52] More than 40% of new chemical entities (NCE) approved by FDA in 2018 contain one or more fluorine atoms.[53] This research represents a case study highlighting the significant impact of fluorine substitution pattern on intrinsic potency, metabolite stability and pharmacokinetics properties.

Our work culminated in the advancement of PT2977, a novel HIF-2α inhibitor with excellent *in vitro* potency, pharmacokinetic profile and *in vivo* efficacy in mouse tumor models. The clinical pharmacokinetics of PT2977 demonstrated consistent and significantly higher exposure than PT2385, achieved with much lower dose and once daily dosing. PT2977 also showed encouraging outcomes in patients with advanced renal cell carcinoma in an expansion cohort of fifty-five patients with ccRCC treated at 120 mg q.d. As of January 1, 2019, 12 patients (22%) had a confirmed partial response. Median progression free survival (PFS) was not yet reached in the study with a median follow-up of 9 months, and 36% of patients remained on study at the time of the data cut-off.[50] Data supports continued clinical development with planned PT2977 monotherapy Phase 3 trial. In addition, an international Phase 2 study in patients with VHL Disease is ongoing.

Chemical Synthesis

Preparation of compounds **1**, **7** and **8** has been previously reported.[27] Syntheses of compounds **2, 6, 9-11** and **13** are summarized in Scheme 1. Reduction of ketone **14** by Noyori's asymmetric transfer hydrogenation afforded **6** enantioselectively. Preparation of **2**, **9-11** and **13** began with acetylation of the alcohol in **1**, **6** and **7** followed by benzylic bromination with *N*-bromosuccinimide (NBS) catalyzed by 2,2'-azobis(2-methylpropionitrile) (AIBN). Subsequent treatment of **16** with Ag_2CO_3 or $AgClO_4$ in 1,2-dimethoxyethane and water gave alcohols **17**. Fluorination of the hydroxy groups in **17** followed by deprotection yielded the target compounds. Mixtures of diastereomers were readily separated by chromatography on silica gel, either at the alcohol **17** step or after fluorination.

Scheme 1. Synthesis of 2, 6, 9-11 and 13[a]

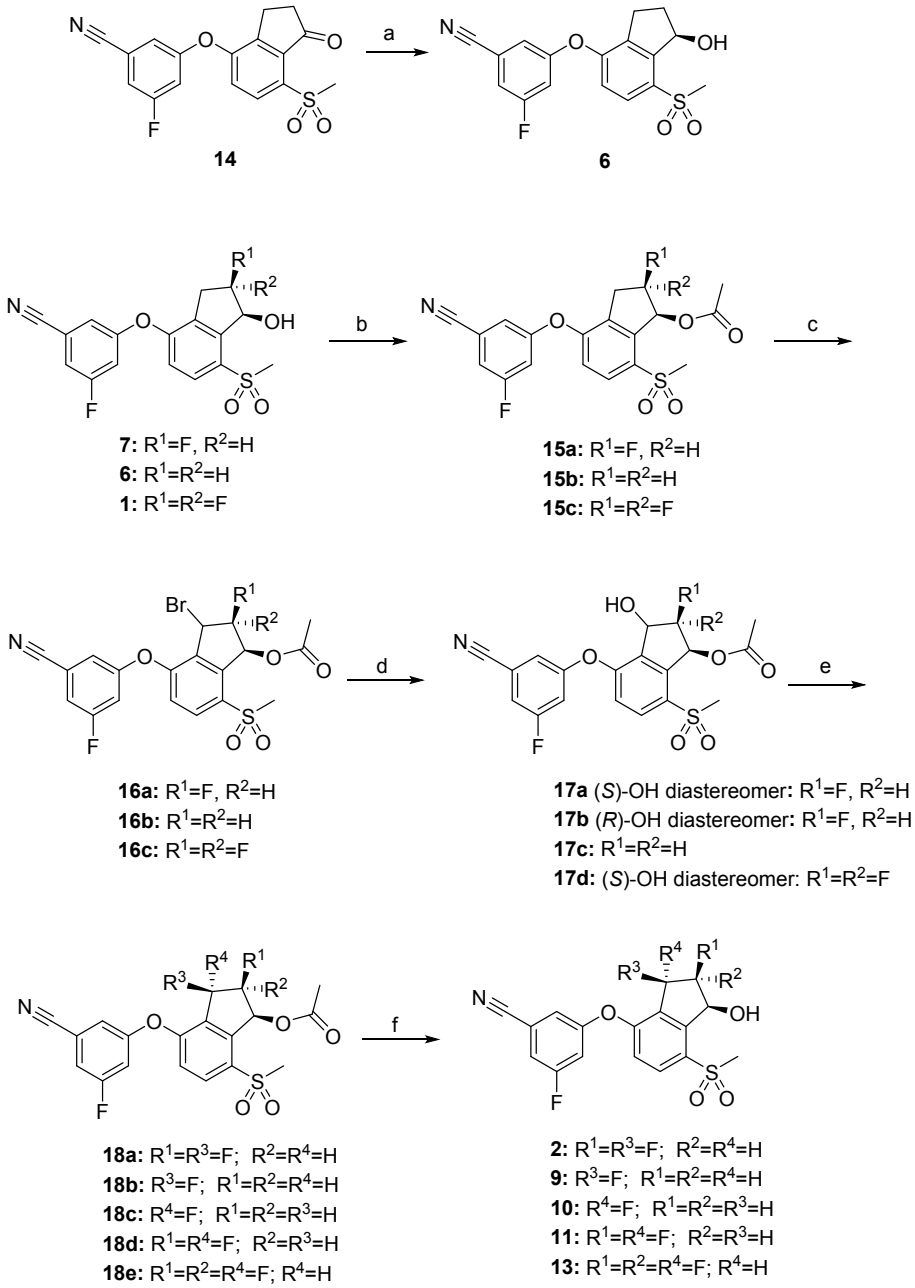

[a]Reagents and conditions: (a) [(*R*,*R*)-Ts-DPEN]RuCl(*p*-cymene), HCO_2H, Et_3N, CH_2Cl_2, rt, 83%; (b) Ac_2O, Et_3N, DMAP, CH_2Cl_2, rt, 61-96%; (c) NBS, AIBN, 1,2-dichloroethane or carbon tetrachloride, 80 °C; (d) Ag_2CO_3 or $AgClO_4$, 1,2-dimethoxyethane, water; (e) DAST, CH_2Cl_2, -78 °C → 0 °C; (f) LiOH, THF, water, rt, 23-86%.

The installation of the benzylic geminal difluoro group in **12** was accomplished by fluorination of the ketone **19**, which was easily obtained by oxidation of the alcohol **17c**. Hydrolysis of the acetate protecting group led to **12** in excellent overall yield (Scheme 2).

Scheme 2. Synthesis of 12[a]

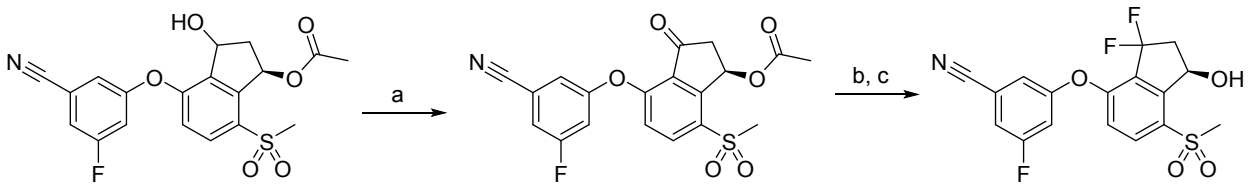

17c **19** **12**

[a]Reagents and conditions: (a) Dess-Martin periodinane, CH_2Cl_2, rt, 88%; (b) 4-(*tert*-butyl)-2,6-dimethylphenyl sulfur trifluoride, hydrogen fluoride pyridine (70%), CH_2Cl_2, rt, 84%; (c) LiOH, THF, water, 0 °C, 86%.

To synthesize the glucuronide metabolites **3** and **20**-**25**, alcohols **1**, **2**, **6**-**9** and **13** were treated with the glucuronosyl donor, 2,3,4-tri-*O*-acetyl-α-*D*-glucuronide methyl ester trichloroacetimidate, in dry DCM using boron trifluoride diethyl etherate or trimethylsilyl trifluoromethanesulfonate as a promoter, produced the corresponding glycosidic coupling products stereoselectively. Subsequent removal of the acetyl protecting groups and the methyl ester under basic conditions in THF afforded the glucuronides (Scheme 3).

Scheme 3. General synthesis of glucuronide metabolites[a]

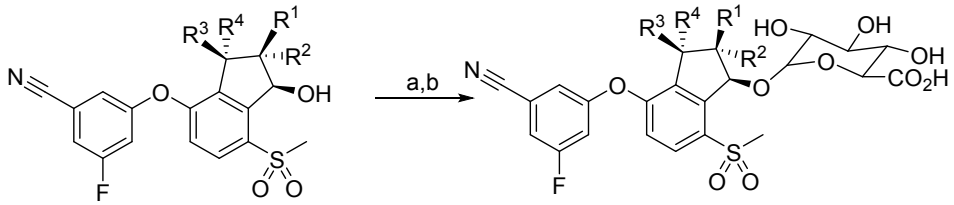

3 (PT2639): R^1=R^2=F, R^3=R^4=H
20 (PT3317): R^1=R^3=F, R^2=R^4=H
21: R^1=R^2=R^3=R^4=H

22: R^1=F, R^2=R^3=R^4=H
23: R^2=F, R^1=R^3=R^4=H
24: R^3=F, R^1=R^2=R^4=H
25: R^1=R^2=R^3=F, R^4=H

[a]Reagents and conditions: (a) 2,3,4-tri-*O*-acetyl-α-*D*-glucuronide methyl ester trichloroacetimidate, boron trifluoride diethyl etherate (Method A) or trimethylsilyl trifluoromethanesulfonate (Method B), CH_2Cl_2, rt; (b) LiOH, THF, water.

EXPERIMENTAL SECTION

General Chemistry: All solvents and reagents were used as obtained. ^1H and ^{19}F analysis of intermediates and exemplified compounds were performed on an Agilent Technologies 400/54 magnet system (operating at 399.85 MHz or 376.24 MHz). Vnmrj VERSION 3.2 software pulse sequences were selected from the default experiment set. Chemical shifts are expressed as δ units using trimethylsilane (TMS) as the external standard (in NMR description, s = singlet, d = doublet, t = triplet, q = quartet, m = multiplet, and br = broad peak).

High performance liquid chromatography (HPLC) coupled to a mass spectrometer (MS) was used to determine the purity of the compounds synthesized. The data confirmed that the target compounds had ≥ 95% of purity. The following analytical method was used to determine chemical purity of final compounds: Agilent 1200 series high performance liquid chromatography (HPLC) system operating in reverse-phase mode coupled to an Agilent 6150 Quadrapole spectrometer using an ESI source, water with 0.1% formic acid (mobile phase A), acetonitrile with 0.1% formic acid (mobile phase B), Agilent ZORBAX Eclipse Plus C18, 1.8 μm, 2.1×50 mm, 40 °C column temperature, 5−95% mobile phase B in 4.0 min, 95% in 2.0 min, 700 μL/min flow rate, UV absorbance detection at 220 and 254 nm. Analyte ions were detected by mass spectrometry in both negative and positive modes (110 – 800 amu scan range, API-ES ionization). For some compounds an additional longer method was also used to assay chemical purity: Agilent 1200 series high performance liquid chromatography (HPLC) system operating in

reverse-phase mode, water with 0.1% formic acid (mobile phase A), acetonitrile with 0.1% formic acid (mobile phase B), Phenomenex Kinetex 2.6 μm C18 100 Å, 30x3.0 mm, 40 °C column temperature, 5−95% mobile phase B in 12.0 min, 95% in 2.0 min, 800 μL/min flow rate, UV absorbance detection at 214 and 254 nm.

Routine chromatographic purification was performed using Biotage Isolera One automated systems running Biotage Isolera One 2.0.6 software (Biotage LLC, Charlotte, NC). Flow rates were the default values specified for the particular column in use. Reverse phase chromatography was performed using elution gradients of water and acetonitrile on KP-C18-HS Flash+ columns (Biotage LLC) of various sizes. Normal phase chromatography was performed using elution gradients of various solvents (e.g. hexanes, ethyl acetate, methylene chloride, methanol, acetone, chloroform, MTBE, etc.). The columns were SNAP Cartridges containing KP-SIL (50 μm irregular particles) or SNAP Ultra (25μm spherical particles) of various sizes (Biotage LLC).

The protocols and procedures involving the care and use of animals for this study were reviewed and approved by the Institutional Animal Care and Use Committee (IACUC) of AAALAC-certified animal facilities.

All patients provided written informed consent. The study protocol was approved by institutional review boards at all participating institutions. The study (NCT02974738) was conducted in accordance with good clinical practice and the Declaration of Helsinki.

Details concerning the SPA assay, luciferase assay, VEGFA secretion assay, in vitro microsomal stability assay, plasma protein binding assay, permeability assay, CYP inhibition assessment, *in*

vivo pharmacokinetic experiments, PK/PD study and *in vivo* efficacy study were described previously.[27]

3-[(1*S*,2*S*,3*R*)-2,3-Difluoro-1-hydroxy-7-methylsulfonyl-indan-4-yl]oxy-5-fluoro-benzonitrile (2). *Step A: Preparation of [(1S,2R)-4-(3-cyano-5-fluoro-phenoxy)-2-fluoro-7-methylsulfonyl-indan-1-yl] acetate (**15a**):* To a stirred solution of 3-fluoro-5-[(1*S*,2*R*)-2-fluoro-1-hydroxy-7-methylsulfonyl-indan-4-yl]oxy-benzonitrile (**7**) (2.00 g, 5.47 mmol) in DCM (27 mL) was added 4-(dimethylamino)pyridine (0.200 g, 1.64 mmol) and triethylamine (1.53 mL, 10.9 mmol). Acetic anhydride (1.00 mL, 10.9 mmol) was added dropwise at 0 °C under nitrogen. The reaction mixture was stirred at ambient temperature overnight. The reaction mixture was diluted with DCM, washed with saturated aqueous $NaHCO_3$ and brine, dried and concentrated. The residue was purified by flash chromatography on silica gel (20-40% EtOAc/hexane) to give [(1*S*,2*R*)-4-(3-cyano-5-fluoro-phenoxy)-2-fluoro-7-methylsulfonyl-indan-1-yl] acetate (1.95 g, 87%). LCMS ESI (+) *m/z* 408 (M+H).

*Step B: Preparation of [(1S,2S)-3-bromo-4-(3-cyano-5-fluoro-phenoxy)-2-fluoro-7-methylsulfonyl-indan-1-yl] acetate (**16a**):* To a stirred solution of [(1*S*,2*R*)-4-(3-cyano-5-fluoro-phenoxy)-2-fluoro-7-methylsulfonyl-indan-1-yl] acetate (**15a**) (1.95 g, 4.79 mmol) in 1,2-dichloroethane (24 mL) was added *N*-bromosuccinimide (NBS) (0.94 g, 5.27 mmol) and 2,2'-azobisisobutyronitrile (AIBN) (8 mg, 0.05 mmol). The reaction mixture was heated at 80 °C for 3 hours. After cooling, the reaction mixture was diluted with DCM, washed with saturated aqueous $NaHCO_3$ and brine, dried and concentrated. The residue was purified by column chromatography on silica gel (20-30% EtOAc/hexane) to give [(1*S*,2*S*)-3-bromo-4-(3-cyano-5-fluoro-phenoxy)-2-fluoro-7-methylsulfonyl-indan-1-yl] acetate (2.10 g, 90%). LCMS ESI (+) *m/z* 486, 488 (M+H).

*Step C: Preparation of [(1S,2R,3S)-4-(3-cyano-5-fluoro-phenoxy)-2-fluoro-3-hydroxy-7-methylsulfonyl-indan-1-yl] acetate (**17a**) and [(1S,2R,3R)-4-(3-cyano-5-fluoro-phenoxy)-2-fluoro-3-hydroxy-7-methylsulfonyl-indan-1-yl] acetate (**17b**):* To stirred solution of [(1*S*,2*S*)-3-bromo-4-(3-cyano-5-fluoro-phenoxy)-2-fluoro-7-methylsulfonyl-indan-1-yl] acetate (**16a**) (2.05 g, 4.22 mmol) in 1,2-dimethoxyethane (28 mL) and water (0.050 mL) was added silver perchlorate hydrate (1.42 g, 6.32 mmol). The reaction mixture was heated at 70 °C for 2 hours. After cooling, the reaction mixture was diluted with EtOAc and filtered through Celite. The filtrate was washed with water and brine, dried and concentrated. The residue was purified by flash chromatography on silica gel (20-50%) to give [(1*S*,2*R*,3*S*)-4-(3-cyano-5-fluoro-phenoxy)-2-fluoro-3-hydroxy-7-methylsulfonyl-indan-1-yl] acetate (0.416 g, 23%) as the less polar product. LCMS ESI (+) *m/z* 441 ($M+NH_4^+$). Further elution with 60% EtOAc/hexane gave [(1*S*,2*R*,3*R*)-4-(3-cyano-5-fluoro-phenoxy)-2-fluoro-3-hydroxy-7-methylsulfonyl-indan-1-yl] acetate (0.580 g, 32 %). LCMS ESI (+) *m/z* 441 ($M+NH_4^+$).

*Step D: Preparation of [(1S,2S,3R)-4-(3-cyano-5-fluoro-phenoxy)-2,3-difluoro-7-methylsulfonyl-indan-1-yl] acetate (**18a**):* To a stirred solution of [(1*S*,2*R*,3*S*)-4-(3-cyano-5-fluoro-phenoxy)-2-fluoro-3-hydroxy-7-methylsulfonyl-indan-1-yl] acetate (**17a**) (416 mg, 0.980 mmol) in DCM (10 mL) was added (diethylamino)sulfur trifluoride (DAST) (0.26 mL, 2.0 mmol) at -78 °C under nitrogen. The reaction mixture was allowed to warm to 0 °C and stirred for 15 minutes. The reaction was quenched by saturated aqueous $NaHCO_3$. The mixture was partitioned between EtOAc and water. The aqueous layer was extracted with EtOAc. The combined organic layers were washed with brine, dried and concentrated. The residue was purified by flash chromatography on silica gel (20-40% EtOAc/hexane) to give [(1*S*,2*S*,3*R*)-4-(3-cyano-5-fluoro-

phenoxy)-2,3-difluoro-7-methylsulfonyl-indan-1-yl] acetate (310 mg, 74%). LCMS ESI (+) *m/z* 426 (M+H).

Step E: *Preparation of 3-[(1S,2S,3R)-2,3-difluoro-1-hydroxy-7-methylsulfonyl-indan-4-yl]oxy-5-fluoro-benzonitrile (**2**):* To a stirred solution of [(*1S*,2*S*,3*R*)-4-(3-cyano-5-fluoro-phenoxy)-2,3-difluoro-7-methylsulfonyl-indan-1-yl] acetate (**18a**) (310 mg, 0.730 mmol) in tetrahydrofuran (9 mL) was added 0.5 N LiOH solution (2.2 mL, 1.1 mmol) at 0 °C under nitrogen. The reaction mixture was allowed to warm to ambient temperature and stirred for 4 hours. The reaction was partitioned between EtOAc and water. The aqueous layer was extracted with EtOAc. The combined organic layers were washed with water and brine, dried and concentrated. The residue was purified by flash chromatography on silica gel (30-50% EtOAc/hexane) to give 3-(1*S*,2*S*,3*R*)-2,3-difluoro-1-hydroxy-7-methylsulfonyl-indan-4-yl]oxy-5-fluoro-benzonitrile (120 mg, 43% yield). LCMS ESI (+) *m/z* 384 (M+H); ^{1}H NMR (400 MHz, $CDCl_3$): δ 8.13 (d, 1H), 7.31-7.25 (m, 1H), 7.23-7.19 (m, 1H), 7.14-7.09 (m, 1H), 7.04 (d, 1H), 6.09-5.91 (m, 1H), 5.87-5.80 (m, 1H), 5.25-5.05 (m, 1H), 3.32 (s, 3H), 2.95 (d, 1H).

General Procedure for Preparation of Glucuronide Metabolites (Method A). (2*S*,3*S*,4*S*,5*R*,6*S*)-6-(((*S*)-4-(3-Cyano-5-fluorophenoxy)-2,2-difluoro-7-(methylsulfonyl)-2,3-dihydro-1*H*-inden-1-yl)oxy)-3,4,5-trihydroxytetrahydro-2*H*-pyran-2-carboxylic acid (3, PT2639). *Step A: Preparation of (2S,3S,4S,5R,6R)-2-(methoxycarbonyl)-6-(2,2,2-trichloro-1-iminoethoxy)tetrahydro-2H-pyran-3,4,5-triyl triacetate:* DCM (13 mL) was dried over powdered 4 Å molecular sieves overnight and then added to 2,3,4-tri-*O*-acetyl-α-*D*-glucuronide methyl ester trichloroacetimidate (1.50 g, 3.13 mmol) and 3-[(1*S*)-2,2-difluoro-1-hydroxy-7-methylsulfonyl-indan-4-yl]oxy-5-fluoro-benzonitrile (**1**) (1.00 g, 2.61 mmol) under nitrogen. The reaction mixture was cooled to 4 °C. Boron trifluoride diethyl etherate (322 μL, 2.61 mmol) was

added dropwise. The reaction mixture was allowed to warm to ambient temperature and stirred for 20 hours. The reaction was concentrated *in vacuo*. The residue was purified by reverse phase chromatography with a gradient of 20% to 80% acetonitrile in water to afford ((2*S*,3*S*,4*S*,5*R*,6*R*)-2-(methoxycarbonyl)-6-(2,2,2-trichloro-1-iminoethoxy)tetrahydro-2*H*-pyran-3,4,5-triyl triacetate (1.50 g, 82% yield). LCMS ESI (–) *m/z* 698 (M–H).

*Step B: Preparation of (2S,3S,4S,5R,6S)-6-(((S)-4-(3-cyano-5-fluorophenoxy)-2,2-difluoro-7-(methylsulfonyl)-2,3-dihydro-1H-inden-1-yl)oxy)-3,4,5-trihydroxytetrahydro-2H-pyran-2-carboxylic acid (**3**):* To a stirred solution of (2*S*,3*S*,4*S*,5*R*,6*R*)-2-(methoxycarbonyl)-6-(2,2,2-trichloro-1-iminoethoxy)tetrahydro-2*H*-pyran-3,4,5-triyl triacetate (1.50 g, 2.14 mmol) in THF (20 mL) was added an aqueous solution of lithium hydroxide monohydrate (0.5 M, 21.4 mL, 10.7 mmol) at 0 °C under nitrogen by syringe. The reaction mixture was stirred at 0 °C for 2 hours. The reaction was diluted with water and extracted with MTBE. The aqueous layer was acidified with 1 N HCl (20 mL) and extracted with EtOAc. The combined organic layers were washed with brine, dried over $MgSO_4$, filtered and concentrated *in vacuo*. The residue was purified by reverse phase chromatography with a gradient of 20% to 80% acetonitrile in water to afford (2*S*,3*S*,4*S*,5*R*,6*S*)-6-(((*S*)-4-(3-cyano-5-fluorophenoxy)-2,2-difluoro- 7-(methylsulfonyl)-2,3-dihydro-1*H*-inden-1-yl)oxy)-3,4,5-trihydroxytetrahydro-2*H*-pyran-2-carboxylic acid (0.80 g, 67% yield). HPLC retention time: 1.28 minutes; LCMS ESI (–) *m/z* 558 (M–H); ^{1}H NMR (400 MHz, CD_3OD): δ 7.96 (d, 1H), 7.46–7.49 (m, 1H), 7.38 (brs, 1H), 7.30 (dt, 1H), 7.17 (d, 1H), 5.87 (d, 1H), 3.89 (d, 1H), 3.18–3.80 (m, 9H); ^{19}F NMR (376 MHz, CD_3OD): δ -103.6 – -102.8 (m, 1F), -108.5 (m, 1F), -117.2 – -116.5 (m, 1F).

Isolation and Characterization of PT2639 from Dog Urine Samples. Six urine samples collected following single p.o. administration of 300 mg/kg or 600 mg/kg PT2385 in male beagle

dogs were combined. The combined urine was adjusted to pH 1 with 1 N HCl. The urine was extracted three times with EtOAc. The combined organic layers were washed with brine, dried over Na_2SO_4, filtered and concentrated *in vacuo*. The residue was purified by reverse phase chromatography with a gradient of 20% to 80% acetonitrile in water to give a beige solid. HPLC retention time: 1.28 minutes; LCMS ESI (–) *m/z* 558 (M–H); ^{1}H NMR (400 MHz, CD3OD): δ 7.96 (d, 1H), 7.46–7.49 (m, 1H), 7.39 (brs, 1H), 7.30 (dt, 1H), 7.17 (d, 1H), 5.88 (d, 1H), 3.88 (d, 1H), 3.18–3.70 (m, 9H); ^{19}F NMR (376 MHz, CD3OD): δ -103.6 – -102.8 (m, 1F), -108.5 (m, 1F), -117.1 – -116.4 (m, 1F). LC-MS and NMR spectroscopic results are in agreement with the chemically synthesized sample.

3-Fluoro-5-[(1*R*)-1-hydroxy-7-methylsulfonyl-indan-4-yl]oxy-benzonitrile (6). Formic acid (1.64 mL, 43.4 mmol) was added slowly to a solution of triethylamine (4.04 mL, 29.0 mmol) in dichloromethane (58 mL) at 0 °C under nitrogen. Solid 3-fluoro-5-(7-methylsulfonyl-1-oxo-indan-4-yl)oxy-benzonitrile (**14**)[27] (5.00 g, 14.5 mmol) was then added followed by the addition of RuCl(*p*-cymene)[(*R*,*R*)-Ts-DPEN] (0.092 g, 0.15 mmol) under nitrogen. The flask was then equipped with septa and a limp balloon to relieve the pressure and the reaction mixture was then placed directly in a 4 °C refrigerator overnight with intermittent swirling and venting. The reaction was allowed to warm to rt and stirred overnight. The reaction mixture was then diluted with dichloromethane, washed with saturate aqueous $NaHCO_3$ and brine, dried and concentrated. The residue was purified by flash chromatography on silica gel (20-50% EtOAc/hexane) to give 3-fluoro-5-[(1*R*)-1-hydroxy-7-methylsulfonyl-indan-4-yl]oxy-benzonitrile (4.18 g, 83% yield). LCMS ESI (-) *m/z* 392 (M+ HCO_2^-); ^{1}H NMR (400 MHz, $CDCl_3$): δ 7.83 (d, 1H), 7.19-7.16 (m, 1H), 7.09-7.07 (m, 1H), 7.01-6.96 (m, 2H), 5.71-5.67 (m, 1H), 3.64 (d, 1H), 3.21 (s, 3H), 3.12-3.02 (m, 1H), 2.84-2.75 (m, 1H), 2.52-2.42 (m, 1H), 2.27-2.18 (m, 1H).

3-Fluoro-5-[(1*R*,3*S*)-3-fluoro-1-hydroxy-7-methylsulfonyl-indan-4-yl]oxy-benzonitrile (9).

*Step A: Preparation of [(1R)-4-(3-cyano-5-fluoro-phenoxy)-3-hydroxy-7-methylsulfonyl-indan-1-yl] acetate (**15b**):* To a stirred solution of 3-fluoro-5-[(1*R*)-1-hydroxy-7-methylsulfonyl-indan-4-yl]oxy-benzonitrile (**6**) (1.05 g, 3.00 mmol) in DCM (29 mL) was added 4-(dimethylamino)pyridine (0.369 g, 3.00 mmol) and triethylamine (0.84 mL, 6.1 mmol). Acetyl chloride (0.43 mL, 6.1 mmol) was added dropwise at 0 °C under nitrogen. The reaction mixture was stirred at ambient temperature for 2 hours. The reaction mixture was diluted with DCM, washed with saturated aqueous $NaHCO_3$ and brine, dried and concentrated. The residue was purified by flash chromatography on silica gel (20-50% EtOAc/hexane) to give [(1*R*)-4-(3-cyano-5-fluoro-phenoxy)-7-methylsulfonyl-indan-1-yl] acetate (0.72 g, 61%). LCMS ESI (-) *m/z* 434 (M+ HCO_2^-).

*Step B: Preparation of [(1R)-3-bromo-4-(3-cyano-5-fluoro-phenoxy)-7-methylsulfonyl-indan-1-yl] acetate (**16b**)*: To a stirred solution of [(1*R*)-4-(3-cyano-5-fluoro-phenoxy)-7-methylsulfonyl-indan-1-yl] acetate (**15b**) (720 mg, 1.85 mmol) in carbon tetrachloride (18 mL) was added *N*-bromosuccinimide (NBS) (362 mg, 2.00 mmol) and 2,2'-azobisisobutyronitrile (AIBN) (3 mg, 0.02 mmol). The reaction mixture was heated at 80 °C for 2 hours. After cooling, the reaction mixture was diluted with DCM, washed with saturated aqueous $NaHCO_3$ and brine, dried and concentrated. The residue was purified by column chromatography on silica gel (10-40% EtOAc/hexanes) to give [(1*R*)-3-bromo-4-(3-cyano-5-fluoro-phenoxy)-7-methylsulfonyl-indan-1-yl] acetate (874 mg, 100%). LCMS ESI (-) *m/z*: 512, 514 (M+ HCO_2^-).

*Step C: Preparation of [(1R)-4-(3-cyano-5-fluoro-phenoxy)-3-hydroxy-7-methylsulfonyl-indan-1-yl] acetate (**17c**):* To a stirred solution of [(1*R*)-3-bromo-4-(3-cyano-5-fluoro-phenoxy)-7-methylsulfonyl-indan-1-yl] acetate (**16b**) (423 mg, 0.906 mmol) in 1,2-dimethoxyethane (5 mL)

and water (2 mL) was added silver carbonate (374 mg, 1.35 mmol). The reaction mixture was stirred at ambient temperature overnight. The mixture was diluted with EtOAc and filtered through Celite. The filtrate was washed with water and brine, dried and concentrated. The crude was used in the next step without further purification. LCMS ESI (-) *m/z* 450 ($M+ HCO_2^-$).

*Step D: Preparation of [(1R,3S)-4-(3-cyano-5-fluoro-phenoxy)-3-fluoro-7-methylsulfonyl-indan-1-yl] acetate (**18b**) and [(1R,3R)-4-(3-cyano-5-fluoro-phenoxy)-3-fluoro-7-methylsulfonyl-indan-1-yl] acetate (**18c**):* To a stirred solution of [(1*R*)-4-(3-cyano-5-fluoro-phenoxy)-3-hydroxy-7-methylsulfonyl-indan-1-yl] acetate (**17c**) (306 mg, 0.750 mmol) in DCM (8 mL) was added (diethylamino)sulfur trifluoride (DAST) (0.20 mL, 1.5 mmol) at 0 °C under nitrogen. The reaction mixture was stirred at 0 °C for 30 minutes. The reaction was quenched by the addition of saturated aqueous $NaHCO_3$. The mixture was partitioned between EtOAc and water. The aqueous layer was extracted with EtOAc. The combined organic layers were washed with brine, dried and concentrated. The residue was purified by column chromatography on silica gel (20-40% EtOAc/hexane) to give [(1*R*,3*S*)-4-(3-cyano-5-fluoro-phenoxy)-3-fluoro-7-methylsulfonyl-indan-1-yl] acetate (144 mg, 47%) and [(1*R*,3*R*)-4-(3-cyano-5-fluoro-phenoxy)-3-fluoro-7-methylsulfonyl-indan-1-yl] acetate (82 mg, 27%). LCMS ESI (+) *m/z* 425 ($M+NH_4^+$).

*Step E: Preparation of 3-fluoro-5-[(1R,3S)-3-fluoro-1-hydroxy-7-methylsulfonyl-indan-4-yl]oxy-benzonitrile (**9**):* To a stirred solution of [(1*R*,3*S*)-4-(3-cyano-5-fluoro-phenoxy)-3-fluoro-7-methylsulfonyl-indan-1-yl] acetate (**18b**) (144 mg, 0.350 mmol) in tetrahydrofuran (3.5 mL) was added 0.5 N LiOH solution (1.41 mL, 0.710 mmol) at 0 °C under nitrogen. The reaction mixture was stirred at rt overnight. The reaction was partitioned between EtOAc and water. The aqueous layer was extracted with EtOAc. The combined organic layers were washed with water and brine, dried and concentrated. The residue was purified by column chromatography on silica gel

(30-60% EtOAc/hexane) to give 3-fluoro-5-[(1*R*,3*S*)-3-fluoro-1-hydroxy-7-methylsulfonyl-indan-4-yl]oxy-benzonitrile (91 mg, 70% yield). LCMS ESI (+) m/z 383 ($M+NH_4^+$); ^1H NMR (400 MHz, $CDCl_3$): δ 8.04-8.01 (m, 1H), 7.25-7.22 (m, 1H), 7.18-7.16 (m, 1H), 7.11-7.06 (m, 1H), 7.00 (d, 1H), 6.09-5.79 (m, 1H), 5.69-5.61 (m, 1H), 3.54 (d, 1H), 3.23 (s, 3H), 2.94-2.80 (m, 1H), 2.52-2.41 (m, 1H).

3-Fluoro-5-[(1*R*,3*R*)-3-fluoro-1-hydroxy-7-methylsulfonyl-indan-4-yl]oxy-benzonitrile (10). **10** was prepared from **18c** by the same procedure described for **9**. LCMS ESI (+) m/z 383 ($M+NH_4^+$); ^1H NMR (400 MHz, $CDCl_3$): δ 8.00 (dd, 1H), 7.25-7.22 (m, 1H), 7.18-7.16 (m, 1H), 7.09-7.06 (m, 1H), 6.99 (d, 1H), 6.35-6.18 (m, 1H), 5.95-5.88 (m, 1H), 4.02 (d, 1H), 3.21 (s, 3H), 2.89-2.73 (m, 1H), 2.58-2.43 (m, 1H).

3-[(1*S*,2*S*,3*S*)-2,3-Difluoro-1-hydroxy-7-methylsulfonyl-indan-4-yl]oxy-5-fluoro-benzonitrile (11). *Step A: Preparation of [(1S,2S,3S)-4-(3-cyano-5-fluoro-phenoxy)-2,3-difluoro-7-methylsulfonyl-indan-1-yl] acetate (**18d**):* To a stirred solution of [(1*S*,2*R*,3*R*)-4-(3-cyano-5-fluoro-phenoxy)-2-fluoro-3-hydroxy-7-methylsulfonyl-indan-1-yl] acetate (**17b**) (28 mg, 0.070 mmol) in dichloromethane (0.7 mL) was added (diethylamino)sulfur trifluoride (DAST) (0.018m L, 0.13 mmol) at 0 °C under nitrogen. The reaction mixture was stirred at 0 °C for 30 minutes. The reaction was quenched by sat. aq. NaHCO3. The mixture was partioned between EtOAc and water. The reaction was quenched by saturated aqueous $NaHCO_3$. The mixture was partitioned between EtOAc and water. The aqueous layer was extracted with EtOAc. The combined organic layers were washed with brine, dried and concentrated. The residue was purified by flash chromatography on silica gel (20-40% EtOAc/hexane) to give [(1*S*,2*S*,3*S*)-4-(3-cyano-5-fluoro-phenoxy)-2,3-difluoro-7-methylsulfonyl-indan-1-yl] acetate (20 mg, 71%). LCMS ESI (+) *m/z* 426 (M+H).

*Step B: Preparation of 3-[(1S,2S,3S)-2,3-difluoro-1-hydroxy-7-methylsulfonyl-indan-4-yl]oxy-5-fluoro-benzonitrile (**11**):* To a stirred solution of [(*1S*,2*S*,3*S*)-4-(3-cyano-5-fluoro-phenoxy)-2,3-difluoro-7-methylsulfonyl-indan-1-yl] acetate (**18d**) (20 mg, 0.047 mmol) in tetrahydrofuran (0.5 mL) was added 0.5 N LiOH solution (0.19 mL, 0.094 mmol) at 0 °C under nitrogen. The reaction mixture was allowed to warm to ambient temperature and stirred for 1 hour. The reaction was partitioned between EtOAc and water. The aqueous layer was extracted with EtOAc. The combined organic layers were washed with water and brine, dried and concentrated. The residue was purified by C18 reversed-phase flash chromatography (20–80% acetonitrile/water gradient) to give 3-(1*S*,2*S*,3*S*)-2,3-difluoro-1-hydroxy-7-methylsulfonyl-indan-4-yl]oxy-5-fluoro-benzonitrile (12 mg, 67% yield). LCMS ESI (+) *m/z* 384 (M+H); ^{1}H NMR (400 MHz, $CDCl_3$): δ 8.04-8.01 (m, 1H), 7.25-7.22 (m, 1H), 7.18-7.16 (m, 1H), 7.11-7.06 (m, 1H), 7.00 (d, 1H), 6.09-5.79 (m, 1H), 5.69-5.61 (m, 1H), 3.54 (d, 1H), 3.23 (s, 3H), 2.94-2.80 (m, 1H), 2.52-2.41 (m, 1H).

3-[(1*R*)-3,3-Difluoro-1-hydroxy-7-methylsulfonyl-indan-4-yl]oxy-5-fluoro-benzonitrile (12).

*Step A: Preparation of [(1R)-4-(3-cyano-5-fluoro-phenoxy)-7-methylsulfonyl-3-oxo-indan-1-yl] acetate (**19**):* To a stirred solution of [(1*R*,3*S*)-4-(3-cyano-5-fluoro-phenoxy)-3-hydroxy-7-methylsulfonyl-indan-1-yl] acetate (**17c**) (366 mg, 0.904 mmol) in DCM (9 mL) was added Dess-Martin periodinane (574 mg, 1.35 mmol). The reaction mixture was stirred at ambient temperature for 1 hour. The reaction mixture was partitioned between EtOAc and saturated aqueous $NaHCO_3$. The aqueous layer was extracted with EtOAc. The combined organic layers were washed with water and brine, dried and concentrated. The crude was purified by flash chromatography on silica gel (10-50% EtOAc/hexane) to give [(1*R*)-4-(3-cyano-5-fluoro-

phenoxy)-7-methylsulfonyl-3-oxo-indan-1-yl] acetate (320 mg, 88%). LCMS ESI (-) *m/z* 402 (M-H).

Step B: Preparation of [(1R)-4-(3-cyano-5-fluoro-phenoxy)-3,3-difluoro-7-methylsulfonyl-indan-1-yl] acetate: To a plastic tube containing [(1*R*)-4-(3-cyano-5-fluoro-phenoxy)-7-methylsulfonyl-3-oxo-indan-1-yl] acetate (**19**) (109 mg, 0.270 mmol) and DCM (1.2 mL) was added 4-(*tert*-butyl)-2,6-dimethylphenyl sulfur trifluoride (115 mg, 0.460 mmol) under nitrogen. Hydrogen fluoride pyridine (70%, 0.020 mL, 0.27 mmol) was added, and the mixture was stirred at ambient temperature for 4 hours. The solvent was removed under reduced pressure. The residue was taken up in EtOAc, washed with saturated aqueous $NaHCO_3$ and brine, dried and concentrated. The residue was purified by flash chromatography on silica gel (10-50% EtOAc/hexane) to give [(1*R*)-4-(3-cyano-5-fluoro-phenoxy)-3,3-difluoro-7-methylsulfonyl-indan-1-yl] acetate (97 mg, 84%). LCMS ESI (+) *m/z* 426 (M+H).

*Step C: Preparation of [(1R)-3,3-difluoro-1-hydroxy-7-methylsulfonyl-indan-4-yl]oxy-5-fluoro-benzonitrile (**12**):* To a stirred solution of [(1*R*)-4-(3-cyano-5-fluoro-phenoxy)-3,3-difluoro-7-methylsulfonyl-indan-1-yl] acetate (**19**) (97 mg, 0.23 mmol) in tetrahydrofuran (1.5 mL) was added 0.5 N LiOH solution (0.68 mL, 0.34 mmol) at 0 °C under nitrogen. The reaction mixture was stirred at 0 °C for 1 hour. The reaction was then partitioned between EtOAc and water. The aqueous layer was extracted with EtOAc. The combined organic layers were washed with water and brine, dried and concentrated. The residue was purified by flash chromatography on silica gel (30-70% EtOAc/hexane) to give [(1*R*)-3,3-difluoro-1-hydroxy-7-methylsulfonyl-indan-4-yl]oxy-5-fluoro-benzonitrile (75 mg, 86%). LCMS ESI (-) *m/z* 428 (M+ HCO_2^-); ^{1}H NMR (400 MHz, $CDCl_3$): δ 8.08 (d, 1H), 7.29-7.23 (m, 1H), 7.19 (brs, 1H), 7.15-7.08 (m, 1H), 7.02 (d, 1H), 5.78-5.70 (m, 1H), 3.89 (d, 1H), 3.23 (s, 3H), 3.17-3.02 (m, 1H), 2.80-2.64 (m, 1H).

3-Fluoro-5-[(1*S*,3*R*)-2,2,3-trifluoro-1-hydroxy-7-methylsulfonyl-indan-4-yl]oxy-benzonitrile (13). *Step A: Preparation of [(1S)-4-(3-cyano-5-fluoro-phenoxy)-2,2-difluoro-7-methylsulfonyl-indan-1-yl] acetate (**15c**):* To a stirred solution of 3-[(1*S*)-2,2-difluoro-1-hydroxy-7-methylsulfonyl-indan-4-yl]oxy-5-fluoro-benzonitrile (**1**) (2.00 g, 5.22 mmol) in dichloromethane (26 mL) was added 4-(dimethylamino)pyridine (0.19 g, 1.6 mmol) and triethylamine (1.45 mL, 10.4 mmol). Acetic anhydride (0.99 mL,10.4 mmol) was added dropwise at 0 °C under nitrogen. The reaction mixture was stirred at rt overnight. The reaction mixture was diluted with DCM, washed with saturated aqueous $NaHCO_3$ and brine, dried and concentrated. The residue was purified by flash chromatography on silica gel (20-50% EtOAc/hexanes) to give [(1*S*)-4-(3-cyano-5-fluoro-phenoxy)-2,2-difluoro-7-methylsulfonyl-indan-1-yl] acetate (2.13 g, 96% yield). LCMS ESI (+) *m/z* 426 (M+H).

*Step B: Preparation of [(1S,3S)-4-(3-cyano-5-fluoro-phenoxy)-2,2-difluoro-3-hydroxy-7-methylsulfonyl-indan-1-yl] acetate (**17d**)*: To a stirred solution of [(1*S*)-4-(3-cyano-5-fluoro-phenoxy)-2,2-difluoro-7-methylsulfonyl-indan-1-yl] acetate (**15c**) (1.00 g, 2.35 mmol) in DCE (24 mL) were added *N*-bromosuccinimide (NBS) (0.460 g, 2.59 mmol) and 2,2'-azobisisobutyronitrile (AIBN) (4 mg, 0.02 mmol). The reaction mixture was heated at 80 °C overnight. After cooling, the reaction mixture was diluted with DCM, washed with saturated aqueous $NaHCO_3$ and brine, dried and concentrated. The crude product was dissolved in 1,2-dimethoxyethane (11 mL) and water (0.11 mL). Silver perchlorate hydrate (0.350 g, 1.55 mmol) was added. The reaction mixture was heated at 70 °C overnight. After cooling, the reaction mixture was diluted with EtOAc and filtered through Celite. The filtrate was washed with water and brine, dried and concentrated. The residue was purified by flash chromatography on silica gel (20-60% EtOAc/hexane) to give [(1*S*,3*S*)-4-(3-cyano-5-fluoro-phenoxy)-2,2-difluoro-3-

hydroxy-7-methylsulfonyl-indan-1-yl] acetate (39 mg, 9% yield). LCMS ESI (+) *m/z* 459 ($M+NH_4^+$).

*Step C: Preparation of [(1S,3R)-4-(3-cyano-5-fluoro-phenoxy)-2,2,3-trifluoro-7-methylsulfonyl-indan-1-yl] acetate (**18e**)*: To a stirred solution of [(1*S*,3*S*)-4-(3-cyano-5-fluoro-phenoxy)-2,2-difluoro-3-hydroxy-7-methylsulfonyl-indan-1-yl] acetate (**17d**) (39 mg, 0.090 mmol) in dichloromethane (1 mL) was added (diethylamino)sulfur trifluoride (DAST) (0.023 mL, 0.18 mmol) at -78 °C under nitrogen. The reaction mixture was allowed to warm to 0 °C and stirred for 15 minutes. The reaction was quenched by saturated aqueous $NaHCO_3$. The mixture was partitioned between EtOAc and water. The aqueous layer was extracted with EtOAc. The combined organic layers were washed with brine, dried and concentrated. The residue was purified by flash chromatography on silica gel (20-40% EtOAc/hexanes) to give [(1*S*,3*R*)-4-(3-cyano-5-fluoro-phenoxy)-2,2,3-trifluoro-7-methylsulfonyl-indan-1-yl] acetate (36 mg, 92% yield). LCMS ESI (+) *m/z* 444 (M+H).

*Step D: Preparation of 3-fluoro-5-[(1S,3R)-2,2,3-trifluoro-1-hydroxy-7-methylsulfonyl-indan-4-yl]oxy-benzonitrile (**13**):* To a stirred solution of [(1*S*,3*R*)-4-(3-cyano-5-fluoro-phenoxy)-2,2,3-trifluoro-7-methylsulfonyl-indan-1-yl] acetate (**18e**) (19 mg, 0.040 mmol) in tetrahydrofuran (0.3 mL) was added 0.5 N LiOH solution (0.13 mL, 0.060 mmol) at 0 °C under nitrogen. The reaction mixture was allowed to warm to ambient temperature and stirred for 2 hours. The reaction was partitioned between EtOAc and water. The aqueous layer was extracted with EtOAc. The combined organic layers were washed with water and brine, dried and concentrated. The residue was purified by flash chromatography on silica gel (20-50% EtOAc/hexanes) to give 3-fluoro-5-[(1*S*,3*R*)-2,2,3-trifluoro-1-hydroxy-7-methylsulfonyl-indan-4-yl]oxy-benzonitrile (4 mg, 23% yield). LCMS ESI (+) *m/z* 419 ($M+NH_4^+$); ^1H NMR (400 MHz, $CDCl_3$): δ 8.14-8.11

(m, 1H), 7.33-7.29 (m, 1H), 7.25-7.23 (m, 1H), 7.16-7.12 (m, 1H), 7.05 (d, 1H), 5.91-5.75 (m, 1H), 5.71-5.65 (m, 1H), 3.39 (d, 1H), 3.25 (s, 3H).

General Procedure for Preparation of Glucuronide Metabolites (Method B). (2*S*,3*S*,4*S*,5*R*,6*S*)-6-(((*S*)-4-(3-Cyano-5-fluorophenoxy)-2,2-difluoro-7-(methylsulfonyl)-2,3-dihydro-1*H*-inden-1-yl)oxy)-3,4,5-trihydroxytetrahydro-2*H*-pyran-2-carboxylic acid (20, PT3317). *Step A: Preparation of (2S,3R,4S,5S,6S)-2-(((1S,2S,3R)-4-(3-cyano-5-fluorophenoxy)-2,3-difluoro-7-(methylsulfonyl)-2,3-dihydro-1H-inden-1-yl)oxy)-6-(methoxycarbonyl)tetrahydro-2H-pyran-3,4,5-triyl triacetate:* Dichloromethane (16 mL) was dried over powdered 4 Å molecular sieves overnight and then added to 2,3,4-tri-*O*-acetyl-α-*D*-glucuronide methyl ester trichloroacetimidate (1.12 g, 2.35 mmol) and 3-(((1*S*,2*S*,3*R*)-2,3-difluoro-1-hydroxy-7-(methylsulfonyl)-2,3-dihydro-1*H*-inden-4-yl)oxy)-5-fluorobenzonitrile (**2**) (0.60 g, 1.57 mmol) under nitrogen. The reaction mixture was cooled to -78 °C. Trimethylsilyl trifluoromethanesulfonate (424 μL, 2.35 mmol) was added dropwise. The reaction mixture was stirred at -78 °C for 30 minutes then the mixture was warmed to ambient temperature and stirred for 7 hours. The reaction was quenched by addition of water, diluted with additional dichloromethane then washed sequentially with saturated $NaHCO_3$ and brine, dried over $MgSO_4$, filtered, and concentrated *in vacuo*. The residue was purified by chromatography on silica gel (10-55% ethyl acetate / hexanes gradient) affording (2*S*,3*R*,4*S*,5*S*,6*S*)-2-(((1*S*,2*S*,3*R*)-4-(3-cyano-5-fluorophenoxy)-2,3-difluoro-7-(methylsulfonyl)-2,3-dihydro-1*H*-inden-1-yl)oxy)-6-(methoxycarbonyl)tetrahydro-2*H*-pyran-3,4,5-triyl triacetate (0.33 g, 30% yield). LCMS ESI (+) *m/z* 700.2 (M+H).

*Step B: Preparation of (2S,3S,4S,5R,6S)-6-(((1S,2S,3R)-4-(3-cyano-5-fluorophenoxy)-2,3-difluoro-7-(methylsulfonyl)-2,3-dihydro-1H-inden-1-yl)oxy)-3,4,5-trihydroxytetrahydro-2H-pyran-2-carboxylic acid (**20**):* A stirred solution of (2*S*,3*R*,4*S*,5*S*,6*S*)-2-(((1*S*,2*S*,3*R*)-4-(3-cyano-5-fluorophenoxy)-2,3-difluoro-7-(methylsulfonyl)-2,3-dihydro-1*H*-inden-1-yl)oxy)-6-(methoxycarbonyl)tetrahydro-2*H*-pyran-3,4,5-triyl triacetate (0.33 g, 0.47 mmol) dissolved in THF (4.7 mL) was cooled to 0 °C. To the solution was added an aqueous solution of lithium hydroxide monohydrate (1.0 M, 2.36 mL, 2.36 mmol) under nitrogen. The reaction mixture was stirred at 0 °C for 3 hours. The reaction was diluted with water, adjusted to pH 4-5 with 0.1 N aqueous HCl, and extracted twice with ethyl acetate. The combined organic layers were washed with brine, dried over $MgSO_4$, filtered and concentrated *in vacuo*. The residue was purified by three sequential C18 reversed-phase flash chromatography runs (20–75% acetonitrile/water gradient) affording (2*S*,3*S*,4*S*,5*R*,6*S*)-6-(((1*S*,2*S*,3*R*)-4-(3-cyano-5-fluorophenoxy)-2,3-difluoro-7-(methylsulfonyl)-2,3-dihydro-1*H*-inden-1-yl)oxy)-3,4,5-trihydroxytetrahydro-2*H*-pyran-2-carboxylic acid (0.082 g, 31% yield). LCMS ESI (–) *m/z* 558 (M–H); ^{1}H NMR (400 MHz, CD_3OD): δ 8.13 (dd, 1H), 7.52-7.49 (ddd, 1H), 7.44-7.42 (m, 1H), 7.36 (dt, 1H), 7.21 (d, 1H), 6.14 (dd, 1H), 6.03 (dd, 1H), 5.29 (m, 1H), 4.92 (d, 1H), 3.88 (d, 1H), 3.53 (t, 1H), 3.46 (t, 1H), 3.37 (s, 3H), 3.23-3.19 (m, 1H).

(2*S*,3*S*,4*S*)-6-(((*R*)-4-(3-Cyano-5-fluorophenoxy)-7-(methylsulfonyl)-2,3-dihydro-1*H*-inden-1-yl)oxy)-3,4,5-trihydroxytetrahydro-2*H*-pyran-2-carboxylic acid (21). 21 was prepared from **6** by the same procedure described for **3**. LCMS ESI (–) *m/z* 522 (M–H); ^{1}H NMR (400 MHz, CD_3OD): δ 7.87 (dd, 1H), 7.54-7.49 (m, 1H), 7.46-7.42 (m, 1H), 7.34-7.32 (m, 1H), 7.22 (d, 1H), 6.06 (d, 1H), 4.74 (d, 1H), 4.01 (d, 1H), 3.60 (t, 1H), 3.52 (t, 1H), 3.30 (s, 3H), 3.23-3.19 (m, 1H), 3.17-3.07 (m, 1H), 2.96-2.86 (m, 1H), 2.54-2.46 (m, 1H), 2.29-2.19 (m, 1H).

(2*S*,3*S*,4*S*)-6-(((1*S*,2*R*)-4-(3-Cyano-5-fluorophenoxy)-2-fluoro-7-(methylsulfonyl)-2,3-dihydro-1*H*-inden-1-yl)oxy)-3,4,5-trihydroxytetrahydro-2*H*-pyran-2-carboxylic acid (22). **22** was prepared from **7** by the same procedure described for **3**. LCMS ESI (–) *m/z* 540 (M–H); ^{1}H NMR (400 MHz, CD_3OD): δ 7.92 (d, 1H), 7.46-7.42 (m, 1H), 7.34-7.31 (m, 1H), 7.27-7.22 (m, 1H), 7.15 (d, 1H), 6.01-5.98 (m, 1H), 5.48-5.28 (m, 1H), 3.88 (d, 1H), 3.54 (t, 1H), 3.44 (t, 1H), 3.33 (s, 3H), 3.32-3.19 (m, 3H).

(2*S*,3*S*,4*S*)-6-(((1*S*,2S)-4-(3-Cyano-5-fluorophenoxy)-2-fluoro-7-(methylsulfonyl)-2,3-dihydro-1*H*-inden-1-yl)oxy)-3,4,5-trihydroxytetrahydro-2*H*-pyran-2-carboxylic acid (23). **23** was prepared from **8** by the same procedure described for **3**. LCMS ESI (–) *m/z* 540 (M–H); ^{1}H NMR (400 MHz, acetone-D6): δ 7.93 (d, 1H), 7.59-7.50 (m, 2H), 7.48-7.40 (m, 1H), 7.27 (d, 1H), 6.03 (d, 1H), 5.64-5.45 (m, 3H), 4.91 (d, 1H), 3.93 (d, 1H), 3.66-3.44 (m, 3H), 3.30 (s, 3H), 3.28-3.22 (m, 1H), 3.20-3.06 (m, 1H).

(2*S*,3*S*,4*S*)-6-(((1*R*,3*S*)-4-(3-cyano-5-fluorophenoxy)-3-fluoro-7-(methylsulfonyl)-2,3-dihydro-1*H*-inden-1-yl)oxy)-3,4,5-trihydroxytetrahydro-2*H*-pyran-2-carboxylic acid (24). **24** was prepared from **9** by the same procedure described for **3**. LCMS ESI (–) *m/z* 540 (M–H); ^{1}H NMR (400 MHz, acetone-D6): δ 8.09 (d, 1H), 7.58 (d, 1H), 7.54-7.51 (m, 1H), 7.47-7.42 (m, 1H), 7.31 (d, 1H), 6.23-6.19 (m, 1H), 6.10-6.00 (m, 1H), 4.81 (d, 1H), 4.04 (d, 1H), 3.63 (t, 1H), 3.54 (t, 1H), 3.38 (s, 3H), 3.34-3.27 (m, 1H), 2.80-2.40 (m, 2H).

(2*S*,3*S*,4*S*)-6-(((1*S*,3*R*)-4-(3-Cyano-5-fluorophenoxy)-2,2,3-trifluoro-7-(methylsulfonyl)-2,3-dihydro-1*H*-inden-1-yl)oxy)-3,4,5-trihydroxytetrahydro-2*H*-pyran-2-carboxylic acid (25). **25** was prepared from **13** by the same procedure described for **20**. LCMS ESI (–) *m/z* 576 (M–H); ^{1}H NMR (400 MHz, acetone-D6): δ 8.19 (d, 1H), 7.71-7.64 (m, 2H), 7.63-7.57 (m, 1H), 7.40

(d, 1H), 6.14-5.93 (m, 2H), 5.13 (d, 1H), 4.15 (d, 1H), 3.66 (t, 1H), 3.59 (t, 1H), 3.37 (s, 3H), 3.37-3.28 (m, 1H).

UGT Phenotyping

The test compound was incubated with a panel of individually-expressed recombinant human UGT enzymes (UGT1A1, UGT1A3, UGT1A4, UGT1A6, UGT1A7, UGT1A8, UGT1A9, UGT1A10, UGT2B7, UGT2B15 and UGT2B17) expressed in baculovirus-infected insect cell membranes (Corning UGT Supersomes). The incubation mixture contained the test compound at a final concentration of 50 μM, expressed UGT (0.2 mg protein/ml), Tris–HCl buffer (pH 7.5), magnesium chloride (10 mM), alamethicin (25 μg/ml) and UDPGA (2 mM). The mixture (without the UDPGA cofactor) was pre-incubated at 37°C for 5 min, after which the reaction was started by the addition of UDPGA.

Incubations were performed at 37°C. Aliquots (100 μl) were collected at 60 min and quenched with two volumes of ice-cold acetonitrile containing an internal standard. The samples were centrifuged at 10,000×*g* at room temperature for 15 min to pellet precipitated proteins. The supernatants were then transferred to clean vials containing 200 μl water and analyzed using liquid chromatography-tandem mass spectrometry (LC-MS/MS). The glucuronide metabolite over internal standard peak area ratio was measured to quantify the glucuronide metabolite formation rate.

Enzyme Kinetic Studies in Human Intestine Microsomes (HIM) and UGT2B17 Supersomes

Similar experimental procedure to UGT phenotyping was used for enzyme kinetics studies of compounds in human intestinal microsomes and UGT2B17 Supersomes, except that a compound concentration range of 2 to 1000 μM was used in the incubations. The absolute glucuronide

metabolite formation rate was measured by LC-MS/MS. The compound concentrations and its corresponding glucuronide metabolite formation rates were fitted to the standard Michaelis-Menten model to obtain the V_{max} and $K_{m.}$ by using Prism (version 6).

Supporting Information

Additional details concerning human MRP2 mediated transport assay of **3**, human MRP2 transport kinetics study of **3**, human P-gp and BCRP transporter studies of **1** and **3**, assessment of **3** in the β-glucuronidase hydrolysis assay, hERG profiling of **2** and safety panel screen of **2** are available.

Molecular formula strings with in vitro activity data (CSV)

AUTHOR INFORMATION

Corresponding Author

*E-mail: rui.xu@pelotontx.com. Phone: 972-629-4033

Present Addresses:

‡ Edgewise Therapeutics, Inc., 3415 Colorado Ave., JSCBB 251E, Boulder, CO 80303

Gilead Sciences, Inc., 333 lakeside Drive, Foster City, CA 94404

Notes

The authors declare no competing financial interests. All authors are employees or former employees of Peloton Therapeutics.

ABBREVIATIONS USED

ARNT, aryl hydrocarbon receptor nuclear translocator; AUC, area under the concentration-time curve; ccRCC, clear cell renal cell carcinoma; CR, complete response; EPO, erythropoietin; HIF,

hypoxia-inducible factor; HIM, human intestine microsomes; HLM, human liver microsomes; HRE, hypoxia-responsive element; MTD, maximum tolerated dose; PFS, progression free survival; PHD, prolyl-hydroxylase; PR, partial response; pVHL, von Hippel-Lindau protein; RP2D, recommended phase 2 dose; SD, stable disease; SPA, scintillation proximity assay; UDPGA, UDP-α-*D*-glucuronic acid; UGT, uridine 5'-diphospho-glucuronosyltransferase; VEGFA, vascular endothelial growth factor A; VHL, von Hippel-Lindau.

REFERENCES

(1) American Cancer Society. https://www.cancer.org/cancer/kidney-cancer/about/key-statistics.html (accessed April 17, 2019).

(2) Choueiri, T.K.; Motzer, R.J. Systemic therapy for metastatic renal-cell carcinoma. *N. Engl. J. Med.* **2017**, *376*, 354-366.

(3) National Cancer Institute. https://seer.cancer.gov/statfacts/html/kidrp.html (accessed April 17, 2019).

(4) Sato, Y.; Yoshizato, T.; Shiraishi, Y.; Maekawa, S.; Okuno, Y.; Kamura, T.; Shimamura, T.; Sato-Otsubo, A.; Nagae, G.; Suzuki, H.; Nagata, Y.; Yoshida, K.; Kon, A.; Suzuki, Y.; Chiba, K.; Tanaka, H.; Niida, A.; Fujimoto, A.; Tsunoda, T.; Morikawa, T.; Maeda, D.; Kume, H.; Sugano, S.; Fukayama, M.; Aburatani, H.; Sanada, M.; Miyano, S.; Homma, Y.; Ogawa, S. Integrated molecular analysis of clear-cell renal cell carcinoma. *Nat. Genet.* **2013**, *45*, 860-867.

(5) Kaelin, W.G., Jr. Molecular Biology of Kidney Cancer. In Kidney Cancer: Principles and Practice, 2nd ed.; Lara, P.N.; Jonasch, E., Eds.; Springer: Cham, **2015**; pp 31-57.

(6) Shen C.; Kaelin, W.G., Jr. The VHL/HIF axis in clear cell renal cell carcinoma. *Semi. Cancer Biol.* **2013**, *23*, 18-25.

(7) Wang, G. L.; Jiang, B. H.; Rue, E. A.; Semenza, G. L. Hypoxia-inducible factor 1 is a basic-helix-loop-helix-PAS heterodimer regulated by cellular O_2 tension. *Proc. Natl. Acad. Sci. USA* **1995**, *92*, 5510-5514.

(8) Tian, H.; McKnight, S. L.; Russell, D. W. Endothelial PAS domain protein 1 (EPAS1), a transcription factor selectively expressed in endothelial cells. *Genes Dev.* **1997**, *11*, 72-82.

(9) Gu, Y. Z.; Moran, S. M.; Hogenesch, J. B.; Wartman, L.; Bradfield, C. A. Molecular characterization and chromosomal localization of a third alpha-class hypoxia inducible factor subunit, HIF3alpha. *Gene Expr.* **1998**, *7*, 205-213.

(10) Wiesener, M.S.; Jurgensen, J.S.; Rosenberger, C.; Scholze, C.K.; Horstrup, J.H.; Warnecke, C.; Mandriota, S.; Bechmann, I.; Frei, U.A.; Pugh, C.W.; Ratcliffe, P.J.; Bachmann, S.; Maxwell, P.H.; Eckardt, K.U. Widespread hypoxia-inducible expression of HIF-2alpha in distinct cell populations of different organs. *FASEB J.* **2003**, *17*, 271-273.

(11) Rosenberger, C.; Mandriota, S.; Jurgensen, J.S.; Wiesener, M.S.; Horstrup, J.H.; Frei, U.; Ratcliffe, P.J.; Maxwell, P.H.; Bachmann, S.; Eckardt, K.U. Expression of hypoxia-inducible factor-1alpha and -2alpha in hypoxic and ischemic rat kidneys. *J. Am. Soc. Nephrol.* **2002**, *13*, 1721-1732.

(12) Kondo, K.; Klco, J.; Nakamura, E.; Lechpammer, M.; Kaelin, W.G, Jr. Inhibition of HIF is necessary for tumor suppression by the von Hippel-Lindau protein. *Cancer Cell* **2002**, *1*, 237-246.

(13) Maranchie, J.K.; Vasselli, J.R.; Riss, J.; Bonifacino, J.S.; Linehan, W.M.; Klausner, R.D. The contribution of VHL substrate binding and HIF1-alpha to the phenotype of VHL loss in renal cell carcinoma. *Cancer Cell* **2002**, *1*, 247-255.

(14) Kondo, K.; Kim, W.Y.; Lechpammer, M.; Kaelin, W.G., Jr. Inhibition of HIF2α is sufficient to suppress pVHL-defective tumor growth. *PLoS Biol.* **2003**, *1*, 439-444.

(15) Zimmer, M.; Doucette, D.; Siddiqui, N.; Iliopoulos, O. Inhibition of hypoxia-inducible factor is sufficient for growth suppression of VHL-/- tumors. *Mol. Cancer Res.* **2004**, *2*, 89-95.

(16) Mathew, L.; Skuli, N.; Macuj, V.; Lee, S.; Zinn, P.; Sathyan, P.; Imtiyaz, H.; Zhang, Z.; Davuluri, R.; Rao, S.; Venneti, S.; Lal, P.; Lathia, J.; Rich, J.; Keith, B.; Minn, A.; Simon, C. miR-218 opposes a critical RTK-HIF pathway in mesenchymal glioblastoma. *Proc. Natl. Acad. Sci. USA* **2014***, 111*, 291-296

(17) Sathornsumette, S.; Cao, Y.; Marcello, J.; Herndon, J.; McLendon, R.; Desjardins, A.; Friedman, H.; Dewhirst, M.; Vredenburgh, J.; Rich, J. Tumor angiogenic and hypoxic profiles predict radiographic response and survival in malignant astrocytoma patients treated with bevacizumab and ironotecan. *J. Clin. Oncology* **2008**, *26*, 271-278.

(18) Jaakkola, P; Mole, D. R.; Tian,Y.-M.; Wilson, M. I.; Gielbert, J.; Gaskell, S. J.; von Kriegsheim, A.; Hebestreit, H. F.; Mukherji, M.; Schofield, C. J.; Maxwell, P. H.; Pugh, C. W.; Ratcliffe, P. J. Targeting of HIF-alpha to the von Hippel-Lindau ubiquitylation complex by O_2-regulated prolyl hydroxylation. *Science* **2001**, *292*, 468-472.

(19) Bruick R. K., McKnight S. L. A conserved family of prolyl-4-hydroxylases that modify HIF. *Science* **2001**, *294*, 1337-1340.

(20) Kaelin, W. G., Jr.; Ratcliffe, P. J. Oxygen sensing by metazoans: the central role of the HIF hydroxylase pathway. *Mol. Cell* **2008**, *30*, 393-402.

(21) Majmundar, A. J.; Wong W. J.; Simon, M. C. Hypoxia-inducible factors and the response to hypoxic stress. *Mol. Cell* **2010**, *40*, 294-309.

(22) Keith, B.; Johnson, R. S.; Simon, M. C. HIF1α and HIF2α: sibling rivalry in hypoxic tumour growth and progression. *Nat. Rev. Cancer* **2011**, *12*, 9-22.

(23) Scheuermann, T. H.; Tomchick, D. R.; Machius, M.; Guo, Y.; Bruick, R. K.; Gardner, K. H. Artificial ligand binding within the HIF2α PAS-B domain of the HIF2 transcription factor. *Proc. Natl. Acad. Sci. USA* **2009**, *106*, 450-455.

(24) Scheuermann, T. H.; Li, Q.; Ma, H. W.; Key, J.; Zhang, L.; Chen, R.; Garcia, J. A.; Naidoo, J.; Longgood, J.; Frantz, D. E.; Tambar, U. K.; Gardner, K. H.; Bruick, R. K. Allosteric inhibition of hypoxia inducible factor-2 with small molecules. *Nat. Chem. Biol.* **2013**, *9*, 271-276.

(25) Rogers, J. L.; Bayeh, L.; Scheuermann, T. H.; Longgood, J.; Key, J.; Naidoo, J.; Melito, L.; Shokri, C.; Frantz, D. E.; Bruick, R. K.; Gardner, K. H.; MacMillan, J. B.; Tambar, U. K. Development of inhibitors of the PAS-B domain of the HIF-2α transcription factor. *J. Med. Chem.* **2013**, *56*, 1739-1747.

(26) Scheuermann, T. H.; Stroud, D.; Sleet, C. E.; Bayeh, L.; Shokri, C.; Wang, H.; Caldwell, C. G.; Longgood, J.; MacMillan, J. B.; Bruick, R. K.; Gardner, K. H.; Tambar U. K. Isoform-selective and stereoselective inhibition of hypoxia inducible factor-2. *J. Med. Chem.* **2015**, *58*, 5930-5941.

(27) Wehn, P.W.; Rizzi, J.P.; Dixon, D.D.; Grina, J.A.; Schlachter, S.T.; Wang, B.; Xu, R.; Yang, H.; Du, X.; Han, G.; Wang, K.; Cao, Z.; Cheng, T.; Czerwinski, R.M.; Goggin, B.S.; Huang, H.; Halfmann, M.M.; Maddie, M.A.; Morton, E.L.; Olive, S.R.; Tan, H.; Xie, S.; Wong, T.; Josey, J.A.; Wallace, E.M. Design and activity of specific hypoxia-inducible factor-2α (HIF-2α) inhibitors for the treatment of clear cell renal cell carcinoma: Discovery of clinical

candidate (*S*)-3-((2,2-difluoro-1-hydroxy-7-(methylsulfonyl)-2,3-dihydro-1H-inden-4-yl)oxy)-5-fluorobenzonitrile (PT2385). *J. Med. Chem.* **2018**, *61*, 9691-9721.

(28) Wallace, E. M.; Rizzi, J. P.; Han, G.; Wehn, P. M.; Cao, Z.; Du, X.; Cheng, T.; Czerwinski, R. M.; Dixon, D. D.; Goggin, B. S.; Grina, J. A.; Halfmann, M. M.; Maddie, M. A.; Olive, S. R.; Schlachter, S. T.; Tan, H.; Wang, B.; Wang, K.; Xie, S.; Xu, R.; Yang, H.; Josey, J. A. A small-molecule antagonist of HIF2α is efficacious in preclinical models of renal cell carcinoma. *Cancer Res.* **2016**, *76*, 5491–5500.

(29) Cho, H.; Du, X.; Rizzi, J. P.; Liberzon, E.; Chakraborty, A. A.; Gao, W.; Carvo, I.; Signoretti, S.; Bruick, R. K.; Josey, J. A.; Wallace, E. M.; Kaelin, W. G. On-target efficacy of a HIF-2α antagonist in preclinical kidney cancer models. *Nature* **2016**, *539*, 107-111.

(30) Chen, W.; Hill, H.; Christie, A.; Kim, M. S.; Holloman, E.; Pavia-Jimenez, A.; Homayoun, F.; Ma, Y.; Patel, N.; Yell, P.; Hao, G.; Yousuf, Q.; Joyce, A.; Pedrosa, I.; Geiger, H.; Zhang, H.; Chang, J.; Gardner, K. H.; Bruick, R. K.; Reeves, C.; Hwang, T. H.; Courtney, K.; Frenkel, E.; Sun, X.; Zojwalla, N.; Wong, T.; Rizzi, J. P.; Wallace, E. M.; Josey, J. A.; Xie, Y.; Xie, X.-J.; Kapur, P.; McKay, R. M.; Brugarolas, J. Targeting renal cell carcinoma with a HIF-2 antagonist. *Nature* **2016**, *539*, 112–117.

(31) Courtney, K. D.; Infante, J. R.; Lam, E. T.; Figlin, R. A.; Rini, B. I.; Brugarolas, J.; Zojwalla, N. J.; Wang, K.; Wallace, E.; Josey, J. A.; Choueiri, T. K. Phase I dose escalation trial of PT2385, a first-in-class hypoxia inducible factor-2α antagonist in patients with previously treated advanced clear cell renal cell carcinoma. *J. Clin. Oncol.* **2018**, *36*, 867-874.

(32) Amidon, G. L.; Lennern€as, H.; Shah, V. P.; Crison, J. R. A. Theoretical basis for a biopharmaceutic drug classification: The correlation of in vitro drug product dissolution and in vivo bioavailability. *Pharm. Res.* **1995**, *12*, 413–420.

(33) Turgeon, D.; Carrier, J.S.; Chouinard, S.; Bélanger, A. Glucuronidation activity of the UGT2B17 enzyme toward xenobiotics. *Drug Metab. Dispos*. **2003**, *31*, 670–676.

(34) Ohno, S.; Nakajin, S. Determination of mRNA expression of human UDP glucuronosyltransferases and application for localization in various human tissues by real-time reverse transcriptase-polymerase chain reaction. *Drug Metab. Dispos.* **2009**, *37*, 32–40.

(35) Zhang, H.; Basit, A.; Busch, D.; Yabut, K.; Bhatt, D.K.; Drozdzik, M.; Ostrowski, M.; Li, A.; Collins, C.; Oswald, S.; Prasad, B. Quantitative characterization of UDP-glucuronosyltransferase 2B17 in human liver and intestine and its role in testosterone first-pass metabolism. *Biochem. Pharmacol.* **2018**, *156*, 32-42.

(36) Sato, Y.; Nagata, M.; Tetsuka, K.; Tamura, K.; Miyashita, A.; Kawamura, A.; Usui, T. Optimized methods for targeted peptide-based quantification of human uridine 5'-diphosphate-glucuronosyltransferases in biological specimens using liquid chromatography-tandem mass spectrometry. *Drug Metab. Dispos.* **2014**, *42*, 885–889.

(37) McCarroll, S.A.; Hadnott, T.N.; Perry, G.H.; Sabeti, P.C.; Zody, M.C.; Barrett, J.C.; Dallaire, S.; Gabriel, S.B.; Lee, C.; Daly, M.J.; Altshuler, D.M. Common deletion polymorphisms in the human genome. *Nat. Genet.* **2006**, *38*, 86-92.

(38) Bhatt, D.K.; Basit, A.; Zhang, H.; Gaedigk, A.; Lee, S.; Claw, K.G.; Mehrotra, A.M.; Chaudhry, A.S.; Pearce, R.E.; Gaedigk, R.; Broeckel, U.; Thornton, T.A.; Nickerson, D.A.;

Schuetz, E.G.; Amory, J.K.; Leeder, J.S.; Prasad, B. Hepatic abundance and activity of androgen- and drug-metabolizing enzyme UGT2B17 are associated with genotype, age, and sex. *Drug Metab. Dispos.* **2018**, *46*, 888-896.

(39) Wang, Y.H.; Trucksis, M.; McElwee, J.J.; Wong, P.H.; Maciolek, C.; Thompson, C.D.; Prueksaritanont, T.; Garrett, G.C.; Declercq, R.; Vets, E.; Willson, K.J.; Smith, R.C.; Klappenbach, J.A.; Opiteck, G.J.; Tsou, J.A.; Gibson, C.; Laethem, T.; Panorchan, P.; Iwamoto, M.; Shaw, P.M.; Wagner, J.A.; Harrelson, J.C. UGT2B17 genetic polymorphisms dramatically affect the pharmacokinetics of MK-7246 in healthy subjects in a first-in-human study. *Clin. Pharmacol. Ther.* **2012**, *92*, 96-102.

(40) Ge, S.; Tu, Y.; Hu, M. Challenges and opportunities with predicting in vivo phase II metabolism via glucuronidation from in Vitro Data. *Curr. Pharmacol. Rep.* **2016**, *2*, 326–338.

(41) Peng, J.; Lu, J.; Shen, Q.; Zheng, M.; Luo X.; Zhu, W.; Jiang, H.; Chen, K. In silico site of metabolism prediction for human UGT-catalyzed reactions. *Bioinformatics* **2014**, *30*, 398-405.

(42) Kerdpin, O.; Mackenzie, P.I.; Bowalgaha, K.; Finel, M.; Miners, J.O. Influence of N-terminal domain histidine and proline residues on the substrate selectivities of human UDP-glucuronosyltransferase 1A1, 1A6, 1A9, 2B7, and 2B10. *Drug Metab. Dispos.* **2009**, *37*, 1948-1955.

(43) Sorich, M.J.; McKinnon, R.A.; Miners, J.O.; Smith, P.A. The importance of local chemical structure for chemical metabolism by human uridine 5-diphosphate-glucuronosyltransferase. *J. Chem. Inf. Model.* **2006**, *46*, 2692-2697.

(44) Singh, S. K.; Das, A. The n → π* interaction: a rapidly emerging non-covalent interaction. *Phys. Chem. Chem. Phys*. **2015**, *17*, 9596-9612.

(45) Graton, J.; Wang, Z.; Brossard, A.-M.; Goncalves Monteiro, D.; Le Questel, J.-Y.; Linclau, B. An unexpected and significantly lower hydrogen-bond-donating capacity of fluorohydrins compared to nonfluorinated alcohols. *Angew. Chem. Int. Ed.* **2012**, *51*, 6176-6180.

(46) Keddie, N.S.; Slawin, A.M.Z.; Lebl, T.; Philp, D.; O'Hagan, D. All-cis 1,2,3,4,5,6-hexafluorocyclohexane is a facially polarized cyclohexane. *Nature Chemistry* **2015**, *7*, 483–488.

(47) Böhm, H.J.; Banner, D.; Bendels, S.; Kansy, M.; Kuhn, B.; Müller, K.; Obst-Sander, U.; Stahl, M. Fluorine in medicinal chemistry. *ChemBioChem* **2004**, *5*, 637−643.

(48) Zhao, Q.; Manning, J.R.; Sutton, J.; Costales, A.; Sendzik, M.; Shafer, C.M.; Levell, J.R.; Liu, G.; Caferro, T.; Cho, Y.S.; Palermo, M.; Chenail, G.; Dooley, J.; Villalba, B; Farsidjani, A.; Chen, J.; Dodd, S.; Gould, T.; Liang, G.; Slocum, K.; Pu, M.; Firestone, B.; Growney, J.; Heimbach, T.; Pagliarini, R. Optimization of 3-pyrimidin-4-yl-oxazolidin-2-ones as orally bioavailable and brain penetrant mutant IDH1 inhibitors. *ACS Med. Chem. Lett.* **2018**, *11*, 746-751.

(49) Papadopoulos, K.P.; Jonasch, E.; Zojwalla, N.J.; Wang, K.; Bauer, T.M. A first-in-human phase 1 dose-escalation trial of the oral HIF-2a inhibitor PT2977 in patients with advanced solid tumors. *J. Clin. Oncol.* **2018,** *36*, suppl, 2508-2508.

(50) Choueiri, T.K.; Plimack, E.R.; Bauer, T.M.; Merchan, J.R.; Papadopoulos, K.P.; McDermott, D.F.; Michaelson, M.D.; Appleman, L.J.; Zojwalla, N.P.; Jonasch, E. A First-in-human Phase 1/2 Trial of the Oral HIF-2α Inhibitor PT2977 in Patients with Advanced RCC. 14th European International Kidney Cancer Symposium, Dubrovnik, Croatia. March 29-30, 2019.

(51) Gillis,E.P.; Eastman, K.J.; Hill, M.D.; Donnelly, D.J.; Meanwell, N.A. Applications of fluorine in medicinal chemistry. *J. Med. Chem.* **2015**, *58*, 8315−8359.

(52) Meanwell, N.A. Fluorine and fluorinated motifs in the design and application of bioisosteres for drug design. *J. Med. Chem.,* **2018**, *61*, 5822–5880.

(53) de la Torre, B.G.; Albericio, F. The pharmaceutical industry in 2018. An analysis of FDA drug approvals from the perspective of molecules. *Molecules*, **2019**, *24*, 809.

Table of Contents Graphic

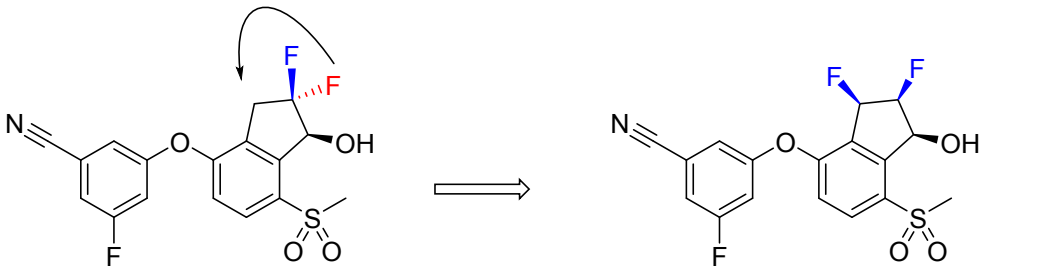

1
(PT2385)

$LogD_{7.4}$: 2.2
VEGFA EC_{50}: 46 nM
Human PPB: 82% bound
Free fraction adjusted EC_{85}: 540 ng/mL

2
(PT2977)

$LogD_{7.4}$: 1.2
VEGFA EC_{50}: 17 nM
Human PPB: 52% bound
Free fraction adjusted EC_{85}: 75 ng/mL